



National University of Science and Technology  
POLITEHNICA BUCHAREST  
DOCTORAL SCHOOL: Mechanical and Mechatronics Engineering

# **Contributions to the study of combustion processes in gas turbines using hydrogen-enriched methane gas mixtures**

**- DOCTORAL THESIS -  
- SUMMARY -**

**Scientific coordinator: Prof. PhD. Eng. Tudor Prisecaru**

**PhD student: Eng. Marius Ștefan Enache**

No. Senate decision..... from .....

**-Bucharest, 2024-**

# TABLE OF CONTENTS

1.	The objectives of the doctoral research.....	4
1.1	The aim of the doctoral research and objectives.....	4
1.2	Analysis of the current stage of development of research in the field.....	6
2.	Experimental campaign.....	8
2.1	Introduction and context.....	9
2.2	Test facility used (campaign 1).....	9
2.3	Technical solutions for noise reduction.....	13
2.4	Thermal parameters and emissions analysis.....	16
2.4.1	Test facility used (campaign 1).....	17
2.4.2	<b>Description of the test facility (campaign 2).....</b>	<b>17</b>
2.4.3	<b>Test configurations.....</b>	<b>17</b>
2.4.4	<b>Flue gas analysis and audio spectra.....</b>	<b>20</b>
2.4.4.1	<b>Experimental campaign records with 60%CH<sub>4</sub>+40%H<sub>2</sub>:.....</b>	<b>20</b>
2.4.4.2	<b>Experimental campaign records with 40%CH<sub>4</sub>+60%H<sub>2</sub>:.....</b>	<b>22</b>
2.4.4.3	<b>Experimental campaign records with 20%CH<sub>4</sub>+80%H<sub>2</sub>:.....</b>	<b>25</b>
2.4.4.4	<b>Experimental campaign records with 100%H<sub>2</sub>:.....</b>	<b>27</b>
2.4.4.5	<b>Acoustic determinations on the experimental installation.....</b>	<b>29</b>
2.4.4.6	<b>Acoustic determinations in the situation of gas combustion of hydrogen-enriched methane gas mixtures on the experimental test rig.....</b>	<b>32</b>
2.5	Experimental campaign (conclusions).....	35
3.	Numerical modeling of reactive turbulent flow.....	36
3.1	Introduction.....	36
3.2	Elements of the kinetics of chemical reactions.....	37
3.2.1	Mechanism of the CH <sub>4</sub> /air reaction.....	37
3.2.2	H <sub>2</sub> /air reaction mechanism.....	37
3.3	Numerical modeling for the new swirler for CH <sub>4</sub> /H <sub>2</sub> mixture operation.....	38
3.4.1	<b>Geometry and computational grid.....</b>	<b>39</b>
3.4.2	<b>Boundary conditions.....</b>	<b>40</b>
4.	Conclusions.....	47
5.	Personal Contributions and Dissemination.....	49
5.1	<b>Personal contributions.....</b>	<b>49</b>
6.	Future research directions.....	51
7.	References:.....	53

## 1. The objectives of the doctoral research

## 1.1 The aim of the doctoral research and objectives

The aim of this doctoral research is to investigate both theoretically and experimentally the effects of hydrogen enrichment of natural gas in the combustion chamber of a gas turbine. At the same time, the doctoral research laid the foundation for the development of an OSIM patent titled: "Combustion Chamber with Premixed Swirl and Primary Dilution" [1], where the author is the main inventor. The patent describes a combustion chamber with premixed swirl and primary dilution used in gas turbines operating on gaseous fuels, especially hydrogen, where the combustible gases consist of mixtures with high combustion speeds. Thus, Figure 1.1 presents the "longitudinal section of the combustion chamber with premixed swirl and primary dilution," and Figure 1.2 shows the innovative concept of the combustion chamber front assembly together with the swirl injector, which is the focus of this study.

The premix, swirl and primary dilution combustion chamber consists of an outer casing, an injection system, a spark plug ignition system and a fire tube, which terminates downstream with a secondary dilution zone.

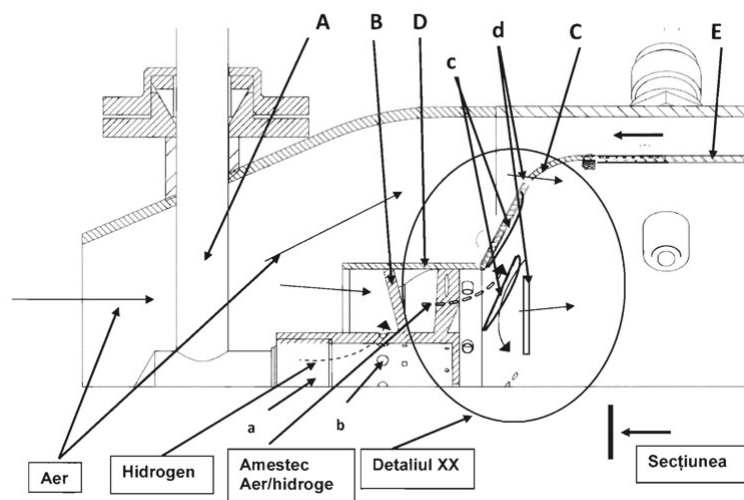


Figure 1.1- Longitudinal section of combustion chamber [6]

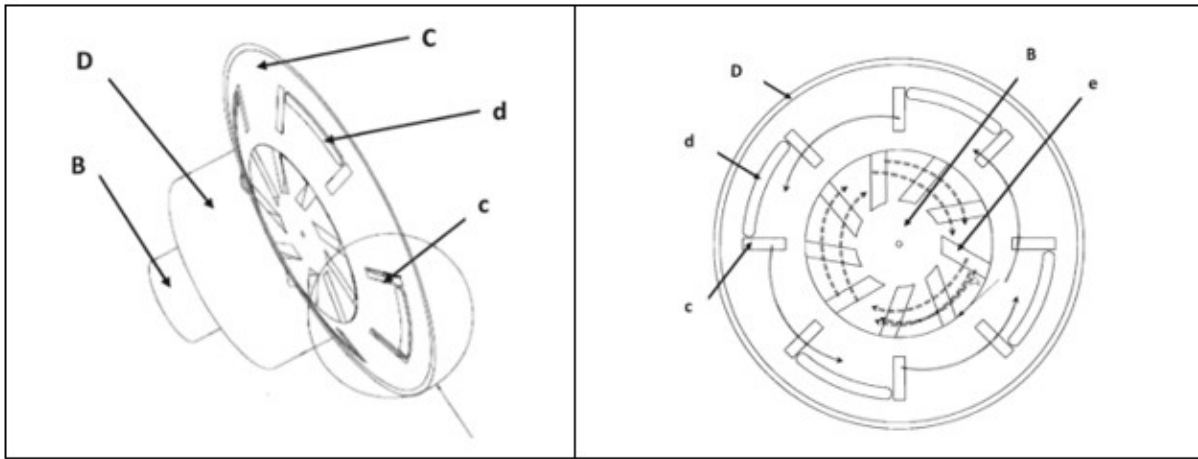


Figure 1.2- Combustion chamber front part with swirl injector [6]

The injection system A supplies gaseous fuel to a swirler B, which is externally provided with helical blades arranged in the axial direction of the flow. These blades form flared helical channels, creating converging nozzles with plane-parallel cross-section, at the exit generating jets at angles to the axial direction, which in turn form swirling jets. The supply of combustible gases is carried out by introducing them through an internal channel of the swirler B and then into the air stream, through holes b located centrally and at the base of each flow channel, in several rows. On the front wall C, which connects the centering piece of the turbulator D to the cylindrical part of the fire tube E, radially arranged swirl slots c are made, which generate swirl jets in the opposite direction to those in the slots e of the turbulator B.

The following objectives are proposed for this doctoral thesis:

- *Analyzing the equations that govern the reactive turbulent flow, as well as the numerical models that facilitate the numerical analysis of these flows;*
- *Realization of three-dimensional numerical simulations of the turbulent flow with heat input (with the ignition of the injector-turbulator concept) in the experimental model regarding methane-hydrogen mixtures in flames with premix, swirl and primary dilution using the ANSYS software, existing in COMOTI;*
- *Starting from the known data and based on the conclusions of the CFD simulations carried out, a new concept of a swirl injector will be developed, which will be integrated into an innovative combustion chamber with premix and swirl for experimental testing.*

- *In addition to pure hydrogen (100% H<sub>2</sub>), hydrogen-methane mixtures (20%H<sub>2</sub>+80%CH<sub>4</sub>, 40%H<sub>2</sub>+60%CH<sub>4</sub>, 80%H<sub>2</sub>+20%CH<sub>4</sub>) will be studied because hydrogen replaces methane as the main component of the fuel.*
- *Attenuation of acoustic waves generated in reactive flows in the situation of using hydrogen-enriched methane gas mixtures as fuel.*
- *Validation of the results of the numerical simulations with the experimental data obtained in the studies presented in this work, as well as with existing experimental data in the specialized literature.*
- *Patenting constructive solutions studied and experienced. Patenting will allow the legal protection of the invention and the opening of opportunities for commercial exploitation through licensing, attracting investment or integration into existing products and technologies, thus strengthening the economic value and scientific contribution of research in the field of combustion systems engineering.*

## **1.2 Analysis of the current stage of development of research in the field**

Reducing CO<sub>2</sub> emissions has become a major priority on the agenda of European institutions, aiming to limit the dramatic effects of climate change on people's daily lives. Increasing fuel combustion efficiency and reducing pollutant emissions, including carbon dioxide emissions, are the dominant trends in the modern energy sector. At the same time, it became obvious that there is no universal solution for reducing the carbon footprint of the energy sector, by simply transitioning industrial energy to renewable sources. The literature data analysis highlights an extensive research and development activity towards the use of methane and hydrogen mixtures as a promising and environmentally friendly fuel characterized by low carbon emissions. The main difference between hydrogen and traditional hydrocarbon-based fuels is the significantly higher burning rate of hydrogen, which, under standard conditions, is at least six times that of methane. Also, hydrogen has much wider concentration limits for flame propagation compared to hydrocarbons. For this reason, in addition to the use of hydrogen as a direct fuel, its use as an additive to traditional fuels, especially compressed natural gas (CNG), is also being intensively explored. A large number of studies have been devoted to the study of the combustion of hydrogen-methane mixtures. Numerical simulations were performed on a combustion chamber using hydrogen-enriched methane gas as fuel by Nam et al [2] to gain a comprehensive understanding of the effect of hydrogen enrichment on turbulent combustion. It was found that as the hydrogen content increased above 11% (by volume), the flame extension angle increased rapidly. NO<sub>x</sub> concentrations increased when hydrogen content was higher than

11 vol%. However, CO emission was not sensitive to the variation of hydrogen concentration. The results showed that the flame structure was slightly influenced by changing the fuel composition. This strongly affected the flow field and therefore the pressure oscillations inside the combustion chamber. When the hydrogen concentration increased, the flame became shorter and thicker, and its effect on the outer recirculation zone was minimized. Glee et al [3] investigate the effectiveness of increasing the fuel injector diameter to extend the mixing limits of hydrogen prior to flashback. The results show that the unmodified burner can support up to 50 vol% hydrogen addition before flashback. By increasing the diameter of the fuel injector, the reduction of primary air is achieved, thus facilitating stable operation for concentrations up to 100% hydrogen. Flame length, visibility and radiant heat transfer properties are all increased as a result of reduced air flow with a trade-off in terms of increased NO<sub>x</sub> emissions. The influence of hydrogen addition on the performance of a counter-current combustor utilizing a methane and air swirl injector was studied by Fu et al [4], both numerically and experimentally. The numerical simulations were performed under certain turbulence intensity conditions for a 100 kW turboshaft engine fueled with a mixture of methane and hydrogen. The results show that an airflow distribution of 50% in the primary zone of the fire tube, 20% in the secondary zone and 30% in the dilution zone leads to an ideal outlet temperature distribution. As the hydrogen ratio increases in the fuel, the outlet temperature decreases and NO<sub>x</sub> pollutant emissions are kept in an ultra-low range. When the hydrogen content by volume exceeds 20%, the addition of hydrogen has a significant impact on the combustion chamber synergy, which favors a uniform outlet temperature distribution and relatively low flow resistance. Abdelhalim et al [5] analyze the stability and combustion characteristics of a layered CH<sub>4</sub>/air flame enriched with hydrogen in a gas turbine combustor model that mimics the Dual Annular Counter-Rotating Counter-Rotating Swirl (DACRS) combustors used in real aeroderivative turbines. The result is that the flame extinction limit remained constant at an equivalence ratio of about 0.5, despite increasing the hydrogen fraction to 20% vol. NO<sub>x</sub> emissions were not affected by hydrogen enrichment up to 20%, but increasing the equivalence ratio favors NO<sub>x</sub> formation, as expected. Marragou et al [6] investigated using a combustion chamber equipped with a coaxial injector, under laboratory conditions, operating regimes and pollutant emissions of partially premixed flames using CH<sub>4</sub>/H<sub>2</sub>/air as fuel. The study shows that the introduction of hydrogen through the central orifice promotes combustion, resulting in low thermal stress on the injector and low NO<sub>x</sub> emissions. The study also points out that reducing the diameter of the central nozzle of the hydrogen injector considerably extends the operating regimes. Flares detach from the injector edge when

the average hydrogen flow velocity is sufficiently high. In this configuration, it has been found that NO<sub>x</sub> emissions remain low even when pure hydrogen is used. Moreover, NO<sub>x</sub> emissions decrease when thermal power increases for a fixed equivalence ratio. The impact of the addition of unmeasured hydrogen on the shape and stabilization mechanisms of a swirled methane/air flame has been analyzed by numerical simulations using the Large Eddy Simulations (LES) method by Laera et al [7]. When hydrogen is added to the mixture, large variations in the Prandtl and Schmidt numbers for N<sub>2</sub> are observed as a function of the local species concentrations, features that are neglected by simplified models. According to the experiments, the classical V-shaped flame is stabilized in the low-velocity region near the flame carrier created by the central recirculation zone (CRZ). Then, hydrogen enrichment of the fuel is achieved by injecting 2% of the CH<sub>4</sub> heat output through a central channel. In this case, both premixed and diffusive flames are present, influencing the flame stabilization and its flame angle. Given the high concentration of H<sub>2</sub> in these regions, the flame stabilization is strongly influenced by the adopted transport models highlighting the importance of using complex transport properties in numerical simulations of hydrogen combustion using the LES method involving hydrogen combustion.

**Keywords: hydrogen, gas turbines, noise reduction, combustion mixtures, CFD.**

## **2. Experimental campaign**

This chapter contains two main experimental campaigns investigating the combustion of methane (CH<sub>4</sub>) enriched with different concentrations of hydrogen (H<sub>2</sub>) in the combustion chamber of a turbo-engine, the combustion being investigated through a quartz tube. The main aim is to analyze the acoustic phenomena and noise produced during combustion, to evaluate carbon monoxide (CO) and nitrous oxide (NO) emissions, and to determine the optimum combustion conditions for various mixtures.

### **2.1 Introduction and context**

The main objectives of the study include analysis of the acoustic behavior of fuel mixtures, evaluation of gaseous emissions, and determination of optimal operating conditions for stable and safe combustion of mixtures with high hydrogen content. The fuel injection was realized by means of the injector-turbulator, which was used in a recent study [8] on the utilization of the effects of adding hydrogen to natural gas in the combustion chamber of a gas turbine. The construction details of this injection and mixing system are shown in Figure 2.1.

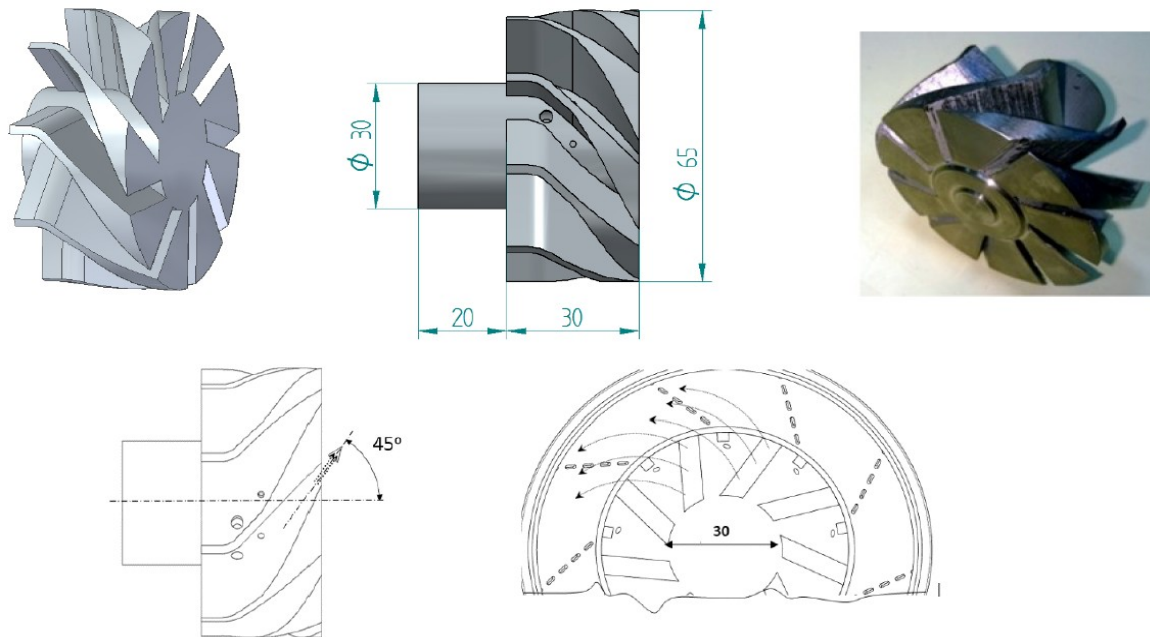


Figure 2.1- Swirl injector [57]

## 2.2 Test facility used (campaign 1)

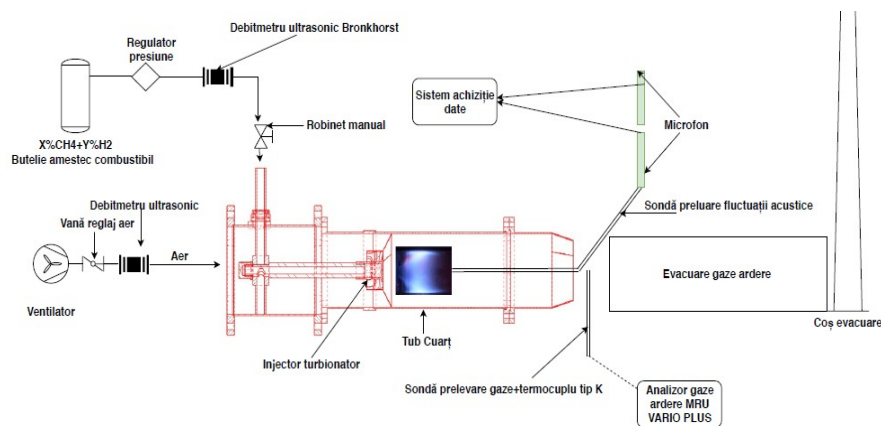


Figure 2.2- Experimental setup (campaign 1)

Measured and processed experimental data are presented upcoming (Table 2.1). The fuel flow rates were subjected to a transformation taking into account the nature of the mixture, which consists of two types of combustible gases.

### Table 2.1 . Experimental data



Nr.Crt	debit aer kg/s	debit CH <sub>4</sub> kg/s	debit CH <sub>4</sub> m <sup>3</sup> /h	Temperatura °C	CO ppm	T stingere °C
1	0.02	0.0007125	0.95	998.4	52	620
2	0.02	0.0006375	0.85	903.6	879	
3	0.02	0.00054	0.72	687.4	2251	
4	0.02	0.0005325	0.71	682.3	2200	
Nr.Crt	debit aer kg/s	debit 90%CH <sub>4</sub> +10%H <sub>2</sub> kg/s (cu factor de corectie)	debit 90%CH <sub>4</sub> +10%H <sub>2</sub> masurat Nm <sup>3</sup> /h	Temperatura °C	CO ppm	T stingere °C
1	0.02	0.000738	5	1023.4	278	540
2	0.02	0.0006585	4.8	939	316	
3	0.02	0.0005604	4	796	1532	
4	0.02	0.0004914	3.6	684.9	1767	
5	0.02	0.0004428	3	602	1800	
		0.0004127	2.8	530.8	1855	
Nr.Crt	debit aer kg/s	debit 80%CH <sub>4</sub> +20%H <sub>2</sub> kg/s (cu factor de corectie)	debit 80%CH <sub>4</sub> +20%H <sub>2</sub> masurat Nm <sup>3</sup> /h	Temperatura °C	CO ppm	T stingere °C
1	0.02	0.0007596	5.8	1020.2	79	526
2	0.02	0.0006512	4.8	932.2	606	
3	0.02	0.0005155	3.8	773.5	1118	
4	0.02	0.0004613	3.4	690.2	1356	
5	0.02	0.0003682	2.8	536	1381	
Nr.Crt	debit aer kg/s	debit 60%CH <sub>4</sub> +40%H <sub>2</sub> kg/s (cu factor de corectie)	debit 60%CH <sub>4</sub> +40%H <sub>2</sub> masurat Nm <sup>3</sup> /h	Temperatura °C	CO ppm	T stingere °C
1	0.02	0.0007234	6.5	1036.9	52	250
2	0.02	0.0005899	5.3	932.2	109	
3	0.02	0.0004897	4.4	805.2	228	
4	0.02	0.0004118	3.7	695.9	550	
5	0.02	0.000345	3.1	589.6	618	
6	0.02	0.0003005	2.7	498.9	628	
7	0.02	0.000256	2.3	353.4	957	
8	0.02	0.0002226	2	289.3	1051	
Nr.Crt	debit aer kg/s	debit 40%CH <sub>4</sub> +60%H <sub>2</sub> kg/s (cu factor de corectie)	debit 40%CH <sub>4</sub> +60%H <sub>2</sub> masurat Nm <sup>3</sup> /h	Temperatura °C	CO ppm	T stingere °C
1	0.02	0.0006821	8	1062.9	14	330
2	0.02	0.0004945	5.8	869	54	
3	0.02	0.0004178	4.9	766.7	92	

Debit aer 0,02kg/s, p\_aer=1,14 bar, taer = 15°C  
 p\_combustibil = 4bar, t\_combustibil 15°C

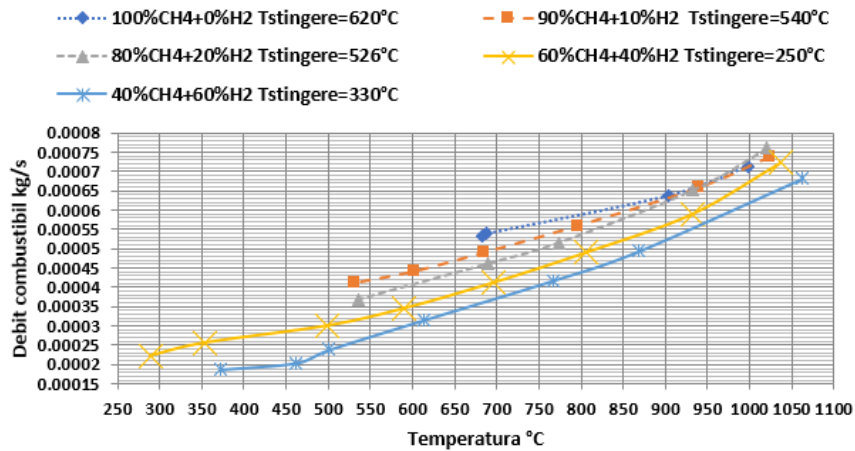


Figure 2.3- Fuel flow values versus flame temperature

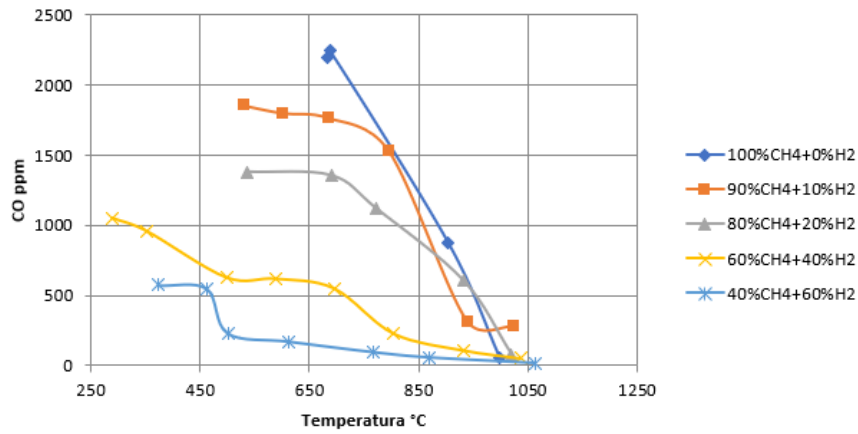


Figure 2.4- Variation of carbon monoxide concentration with temperature.

**Debit aer=0,02kg/s la T=15°C - 113,1 dB**  
**Debit aer=0,02 kg/s+Debit CH4=0,0007125kg/s - 113,4 dB (fară ardere)**

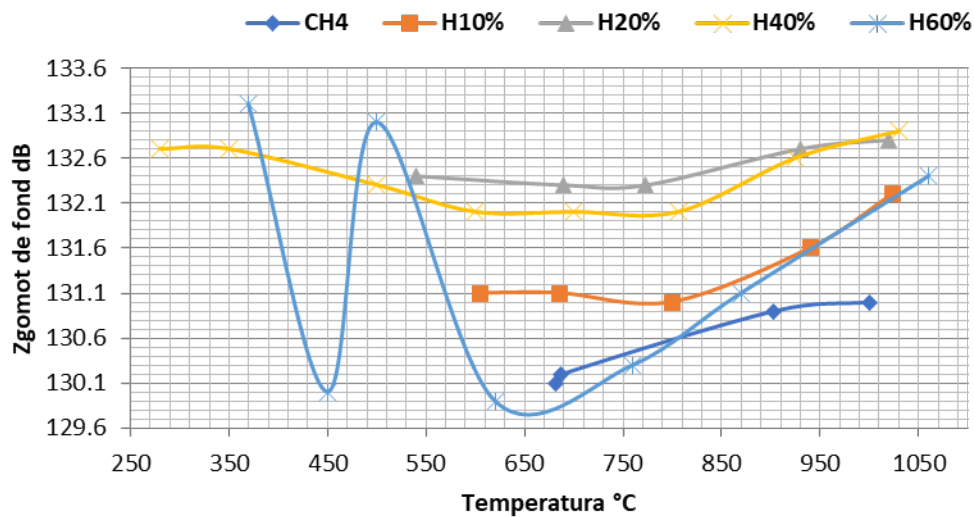


Figure 2.5- Noise measurement

Acoustic signals were captured using a Sirius multi-channel acquisition system supplied by Dewesoft. The following figure shows the frequency domain spectral analyses corresponding to the noise produced by the cold air flow circulation alone compared to the noise produced by the cold air and methane gas flow. It can be observed that the introduction of CH<sub>4</sub> leads to an increase in the mid- and high-frequency noise produced by the turbulent CH<sub>4</sub> jet. In terms of the overall noise level, the methane contribution leads to increase it only by 0.3dB level measured inside the combustion chamber. From the spectral analysis of the signal measured outside the combustion chamber, a spectral component can be observed at the frequency of 24Hz, which originates from the fan operation and corresponds to its operating speed.

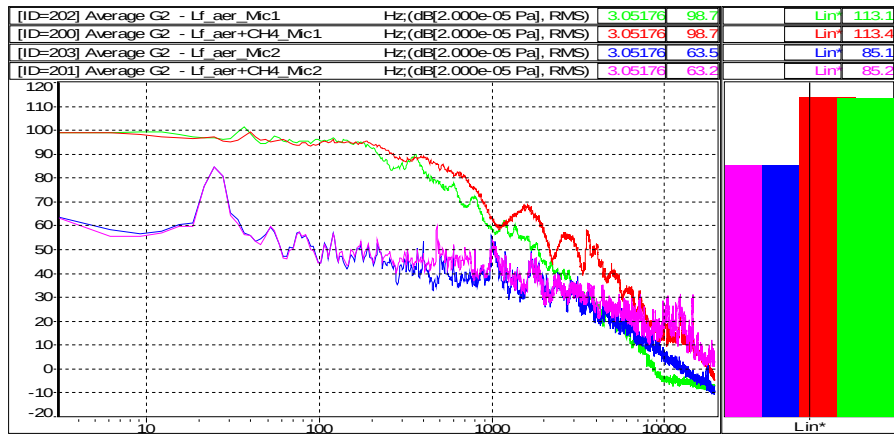


Figure 2.6- Air flow noise compared to air + CH<sub>4</sub> without combustion

In the spectral analysis presented below the noise occurring during methane combustion is highlighted, where an increase in the overall noise level of 16.7dB is observed.

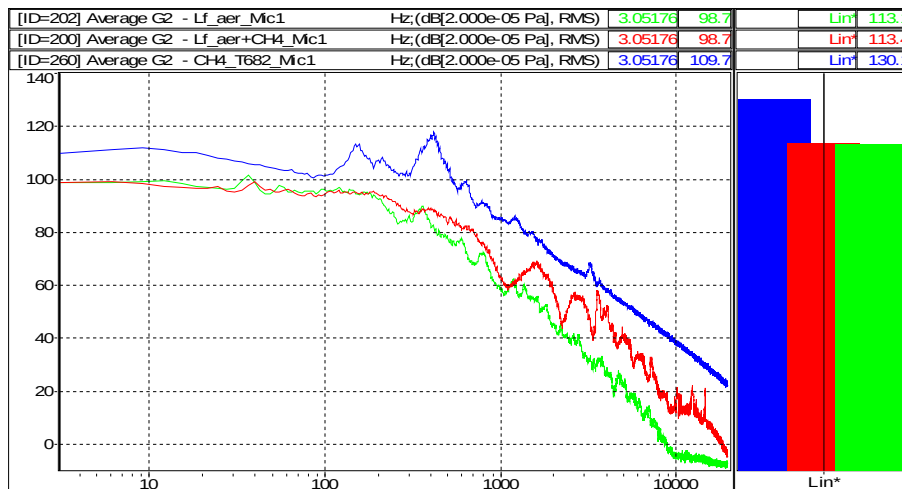


Figure 2.7- Noise produced inside the quartz tube when flowing air, air+methane (cold), air+methane (combustion with 882°C exhaust temperature)

### 2.3 Technical solutions for noise reduction

Several technical solutions have been proposed and tested in order to attenuate the noise produced during the combustion of hydrogen and methane mixtures. One of the most effective methods was the use of a porous copper disk (Fig 2.8) placed in front of the swirler. This disk acts as an acoustic filter that dissipates part of the acoustic energy produced by the combustion. Tests have shown that this disk significantly reduces the noise, especially in the areas where the acoustic frequencies are highest.

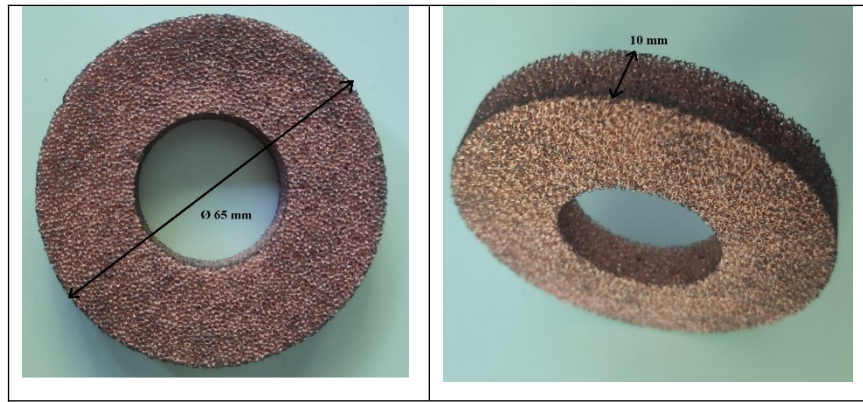


Figure 2.8- Copper disk with pore diameter ranging around 0.5mm with a pore density of 60 pores/inch (equivalence = 81% porosity).

In addition to copper discs, other solutions have been experimented with, such as the addition of an axial jet for (diffusive) flame feed and modification of combustion chamber geometry to optimize air and fuel distribution. In particular, designs incorporating a modified air distribution have reduced hazardous acoustic phenomena and contributed to increased flame stability under operation with hydrogen-rich fuel mixtures.



Figure 2.9- The Swirl injector with central orifice 2 mm in diameter for fuel injection into the combustion chamber.

The following graph (2.10) shows the spectra of the acoustic signals measured at both points for 20%. Two test sessions were performed with H<sub>2</sub>O% maintaining the same thermal thresholds to check the stability of the stand and the generated noise. In the tests at 1020 °C the variation of the sound pressure level at the measuring point in the cold zone is 0.5dB and for the warm zone is 0.1dB.

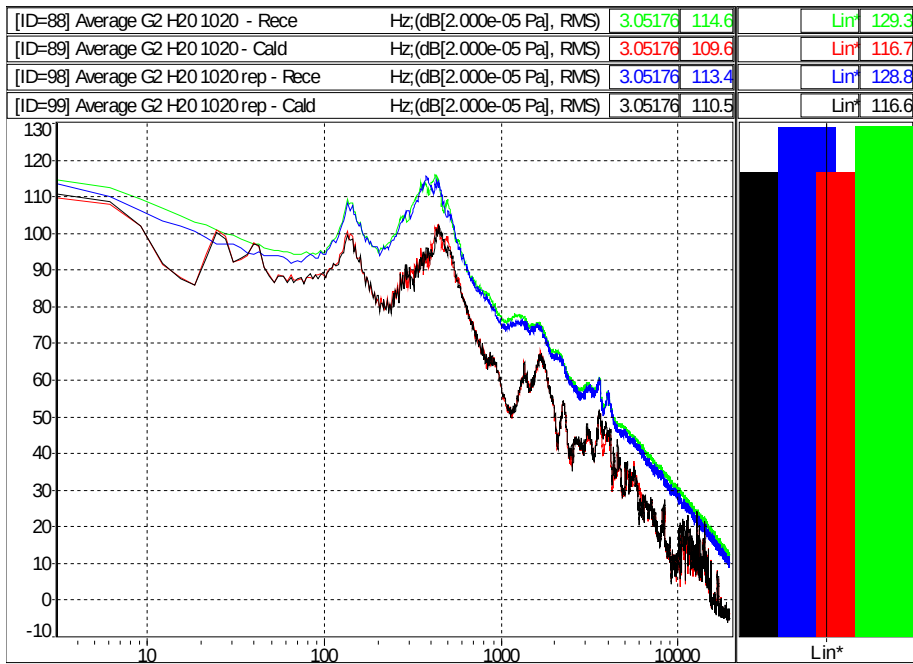


Figure 2.10- Noise variation for 80%CH<sub>4</sub>+20%H<sub>2</sub> burning for 1020°C at exhaust

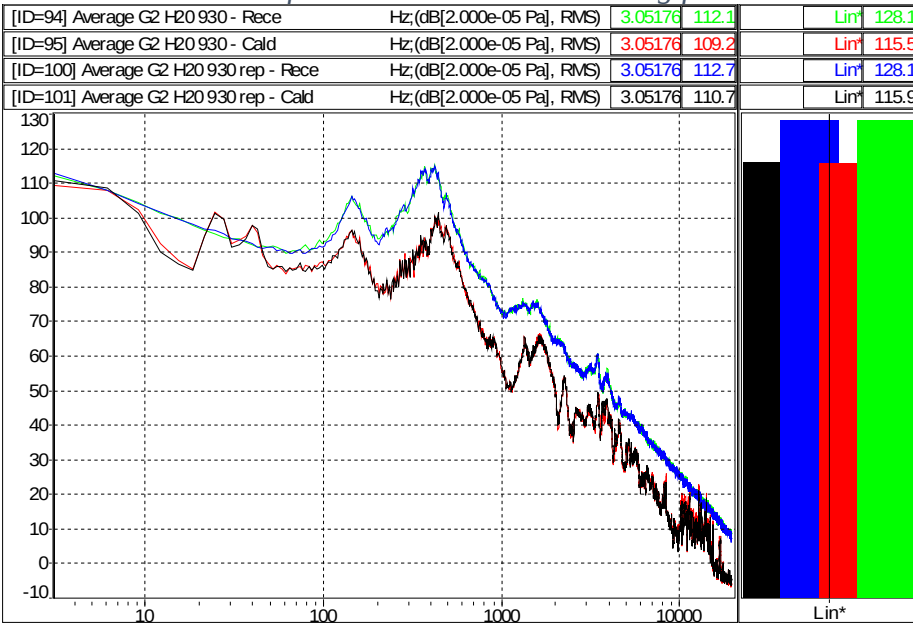


Figure 2.11- Noise variation for 80%CH<sub>4</sub>+20%H<sub>2</sub> burning at 930°C at exhaust

Table 2.2 Results of acoustic measurements

Procent volumic hidrogen+metan	Temperatura °C	Turbionator fără injectie axială	Turbionator cu injectie axială	Turbionator cu injectie axială și disc de cupru
		Nivel presiune acustică dB		
20%H <sub>2</sub> + 80% CH <sub>4</sub>	1020	132,8	131,2	117,9
	770	132,3	128,3	114,1
	536	132,4	127,5	113,4
40%H <sub>2</sub> + 60% CH <sub>4</sub>	1031	132,9	127,5	115,5
	801	132	126,9	114,4
	584	132	127,1	114,1
60%H <sub>2</sub> + 40% CH <sub>4</sub>	1061	132,4	129,5	116,1
	776	136,1	129,9	129,5
	500	135,3	133	127,5

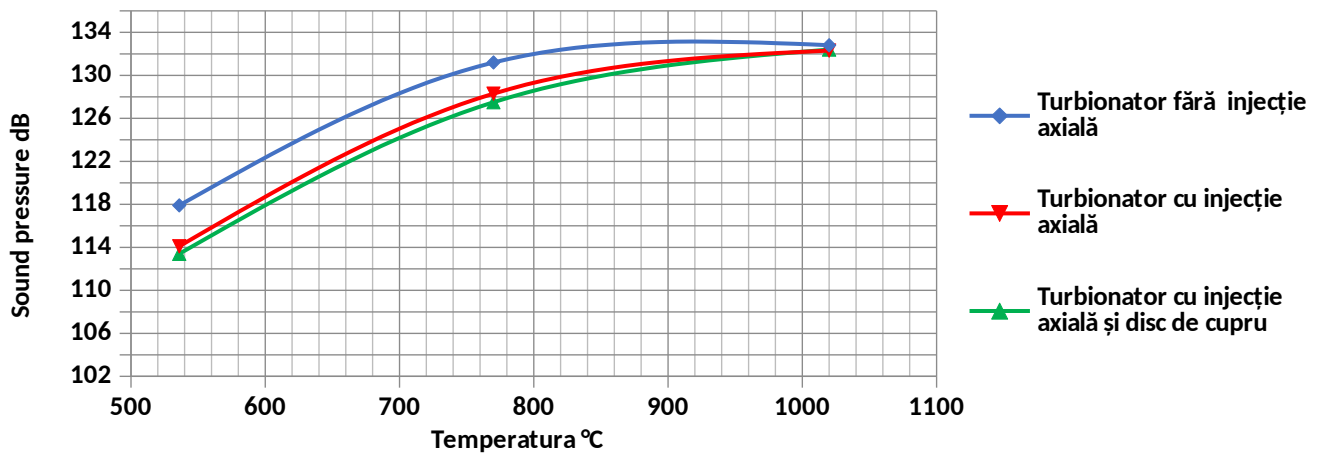


Figure 2.12- Comparative values of session 1 (blue) with session 2 (red and green).

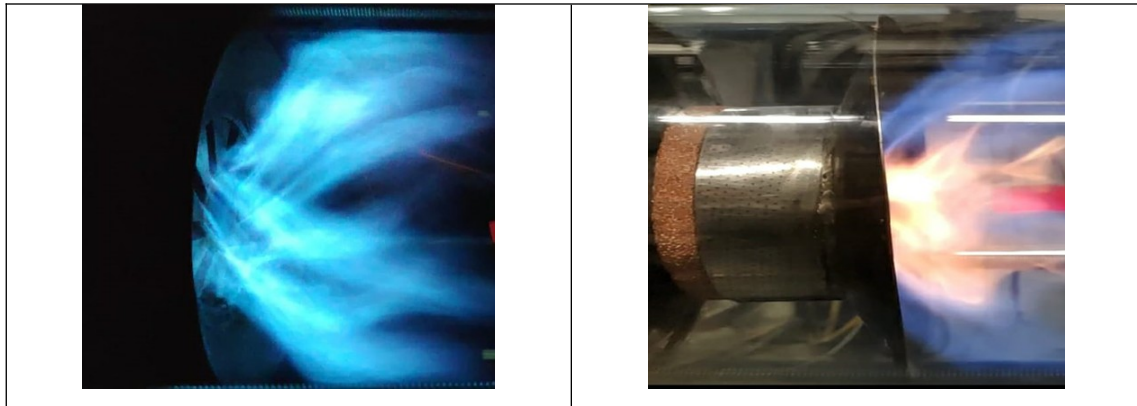


Figure 2.13- Turbulent flame first test session (left), second test session (right)

## 2.4 Thermal parameters and emissions analysis

Flame temperature and CO emissions were monitored during campaign 1 to assess the combustion efficiency and environmental impact of the mixtures. An important result of the study is that mixtures with a higher proportion of hydrogen generate lower CO emissions with increasing hydrogen concentration.

It was also observed that, in general, CO emissions increase significantly when combustion takes place under conditions of oxygen deficiency in the reaction zone or when mixtures are richer in methane. Under these conditions, the incomplete methane oxidation process favors the formation of carbon monoxide.

## 2.4.1 Test facility used (campaign 1)

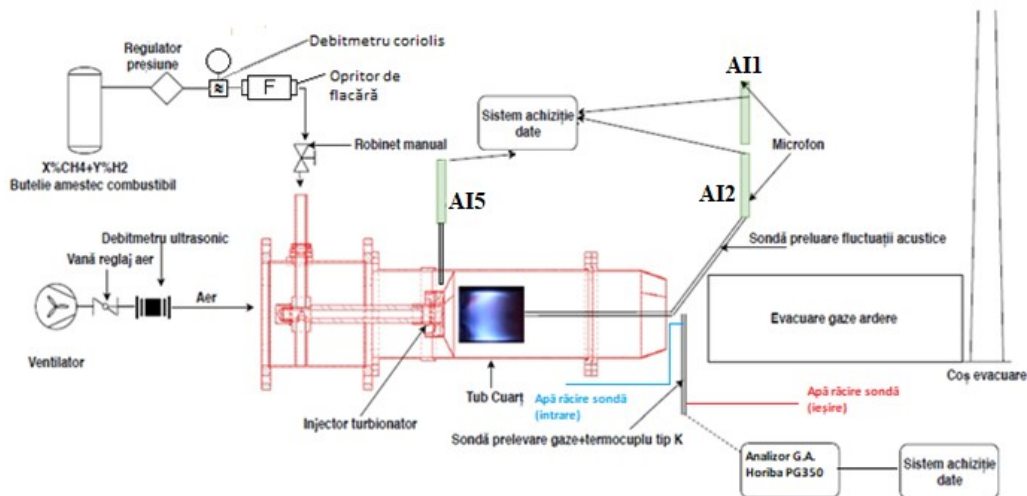


Figure 2.3 - Experimental setup (campaign 2)

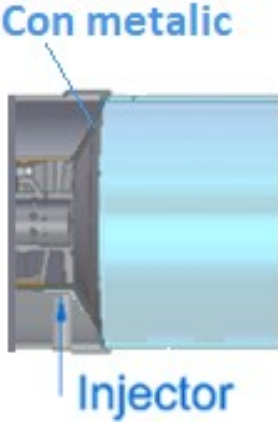
## 2.4.2 Description of the test facility (campaign 2)

The flue gas analysis was performed with a system produced by HORIBA, model PG350, by which NO, CO and CO<sub>2</sub> emissions as well as O<sub>2</sub> concentration were recorded at one second intervals during each test step. The portable measurement system consisted of a portable probe (PSP-4000H), a heated line, a gas sampling system (PSS-5H) and the PG-350 as a gas analyzer.

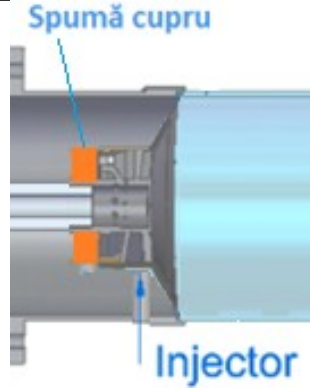
## 2.4.3 Test configurations

The tests were conducted using four fuel injection and fuel-air mixing system configurations in the test volume, each aimed at improving air and fuel distribution, combustion stability, and acoustic performance. The four configurations tested were:

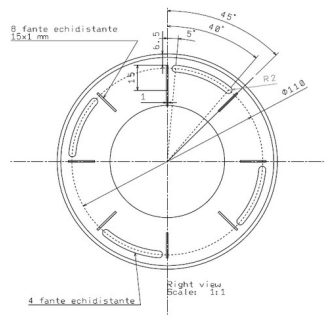
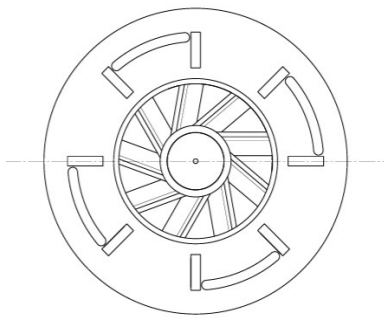
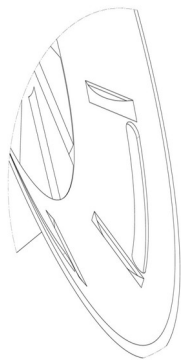
### 2.4.3.1 Configuration 1 [C1] (No copper screen):

 <p>Figure 2.15- ConFigureția 1</p>	<p>In this experimental configuration, the metal cone was made of 0.6 mm thick unperforated sheet of SAE 310S refractory stainless steel which is welded to the supporting section of the quartz tube. All the air will pass strictly through the blades of the swirler, thus avoiding sealing problems at the metal-quartz interface. Also the swirl degree will be increased in the combustion volume due to higher flow velocities</p>
--	---

### 2.4.3.2 Configuration 2 [C2] (With copper screen):

 <p>Figure 2.16- ConFigureția 2</p>	<p>In the next stage, the copper disk was placed to equalize the air flow before entering the turbulator. The acoustic influence of the disk was investigated with the idea that it would act as a porous medium to attenuate acoustic disturbances during combustion. The disk has an outer diameter of 65 mm and a thickness of 10 mm. On this variant mixtures of 40% and 60% H<sub>2</sub> (rest CH<sub>4</sub>) were tested.</p>
---	---

### 2.4.3.3 Configuration 3 [C3] (With swirl slots)

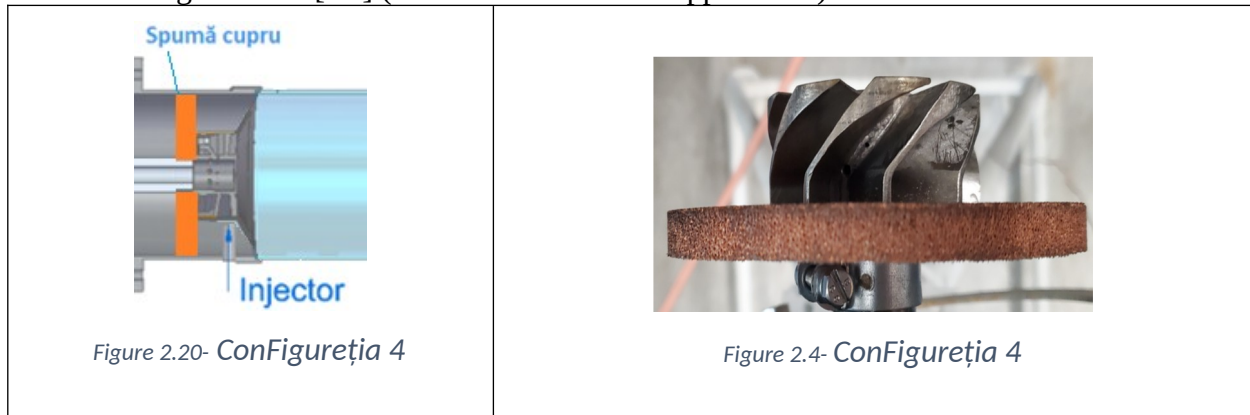
 <p>Figure 2.17 - Configuration 3 (Changes to the front of the combustion chamber)</p>	 <p>Figure 2.18- Configuration 3 (swirl injector - metal cone assembly)</p>	 <p>Figure 2.19- Configuration 3 (Detail of the swirl slots)</p>
---	--	---

Following the observations on the influence of air and fuel jets, approached from the point of view of numerical simulations, a preliminary stage of this study, it was found that a modified air distribution was necessary due to the realization that the simple premixing and swirl



chamber [Patent RO 131144] could not exceed the concentration of 60% H<sub>2</sub> in the fuel mixture because of the noise produced which can become destructive for the whole assembly. Thus, the idea arose, put into practice, executed and experimented, to transform the initial chamber into a "combustion chamber with premixing, swirling and primary dilution" [Patent RO 137923]. On this variant, mixtures with 60%, 80% and 100% H<sub>2</sub> (rest CH<sub>4</sub>) were tested.

#### 2.4.3.4 Configuration 4 [C4] (With swirl slots and copper sieve)



Starting from the construction solution presented previously (Figure 3), a copper disk with an external diameter of 124 mm and thickness of 10 mm was also made for this figure, so that it can be used on the entire surface of the air passage towards the primary zone, both between the blades of the swirler and through the slots made on the sheet metal cone.

## 2.4.4 Flue gas analysis and audio spectra

### 2.4.4.1 Experimental campaign records with 60%CH<sub>4</sub>+40%H<sub>2</sub>:

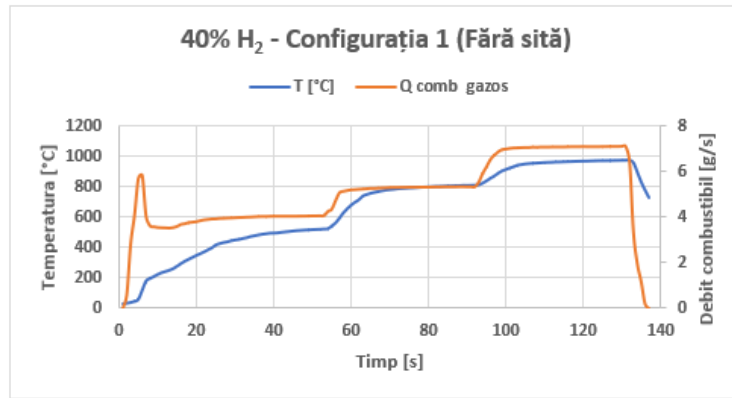


Figure 2.22- Variation during experiments of temperature and fuel flow rate for test configuration 1 at 40% $H_2$  in mixture

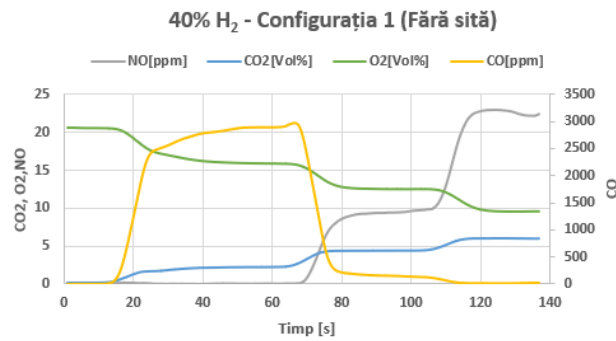


Figure 2.5- Variation during experiments of NO, CO, CO and O<sub>2</sub>, for test configuration number 1 at 40% $H_2$  in the mixture

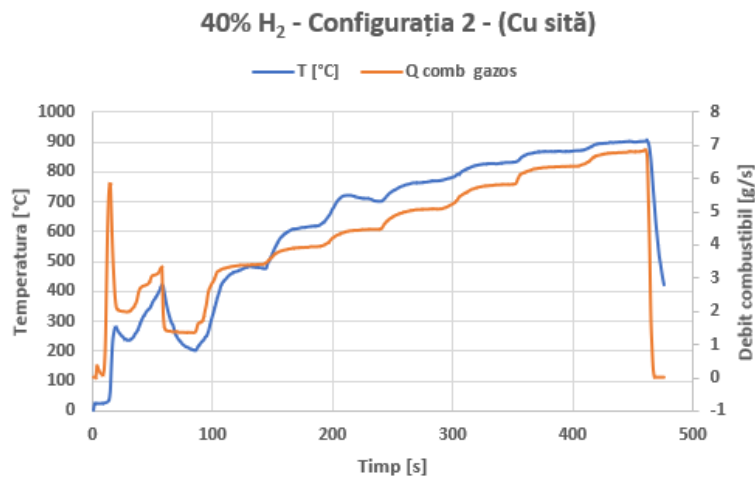


Figure 2.24- Variation during experiments of temperature and fuel flow rate for test configuration number 2 at 40% $H_2$  in mixture

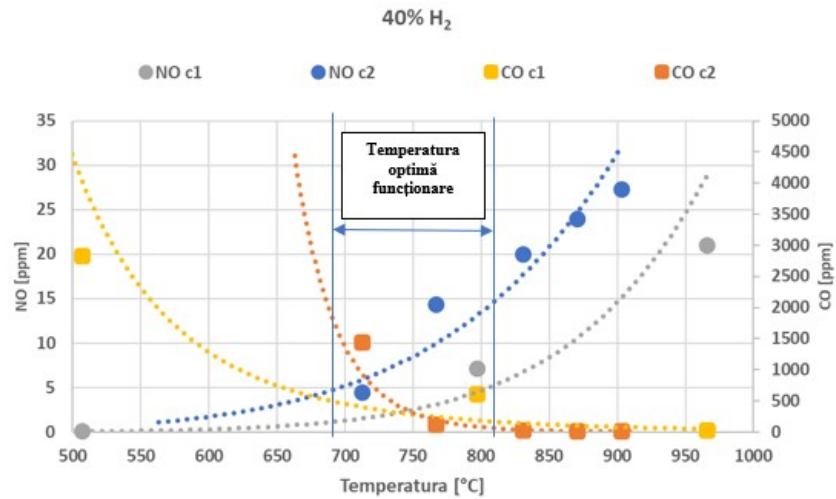


Figure 2.25- Comparison between configuration 1 (without copper sieve) and configuration 2 (with copper sieve) for 40%H<sub>2</sub> in the mixture

For configuration 1 (no copper sieve), the intersection point between the CO and NO emission curves is located on the abscissa at 750°C. For configuration 2 (with copper sieve) the intersection of the CO and NO emission curves on the abscissa is 715°C. There is a slight increasing trend of NO emission values for configuration 2. As far as CO emissions are concerned, there are no noticeable differences between the two configuration, both recording values in the order of hundreds to thousands of units [ppm], a good indicator of a combustion efficiency far from ideal. The low volumetric proportion of hydrogen (40%), translated into a mass fraction of 7.7%, favors high CO emissions, due to the high carbon content of the fuel mixture in relation to the air available for combustion, when these temperature thresholds are reached at a flow rate of 0.02 kg/s air.

### 2.4.4.2 Experimental campaign records with 40%CH<sub>4</sub>+60%H<sub>2</sub>

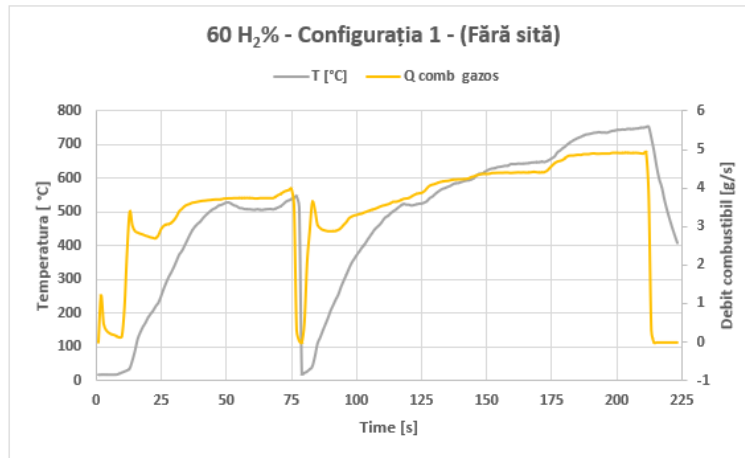


Figure 2.26- Variation during experiments of temperature and fuel flow rate for configuration 1 test at 60%H<sub>2</sub> in mixture

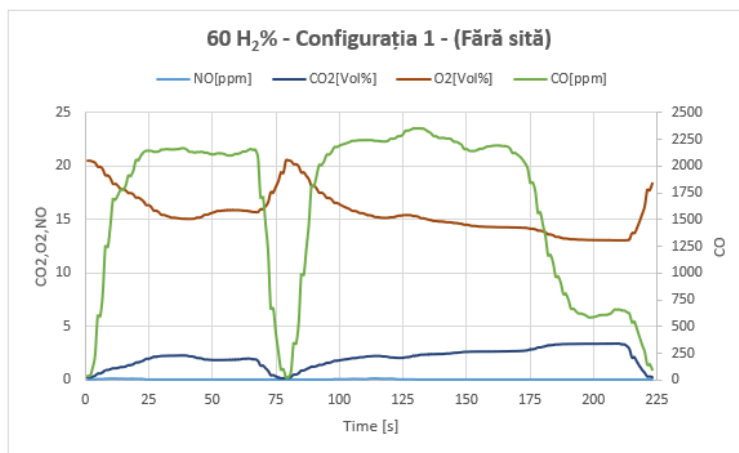


Figure 2.27- Variation during experiments of NO,CO,CO and O<sub>2</sub>, for test configuration 1 at 60%H<sub>2</sub> in the mixture

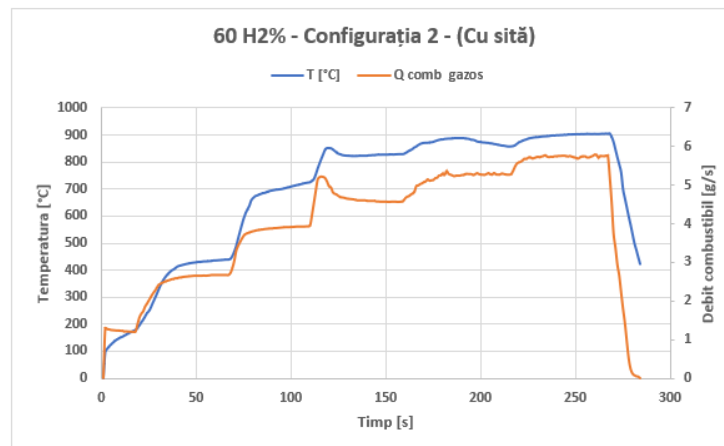


Figure 2.28- Variation during experiments of temperature and fuel flow rate for test configuration 2 at 60%H<sub>2</sub> in the mixture

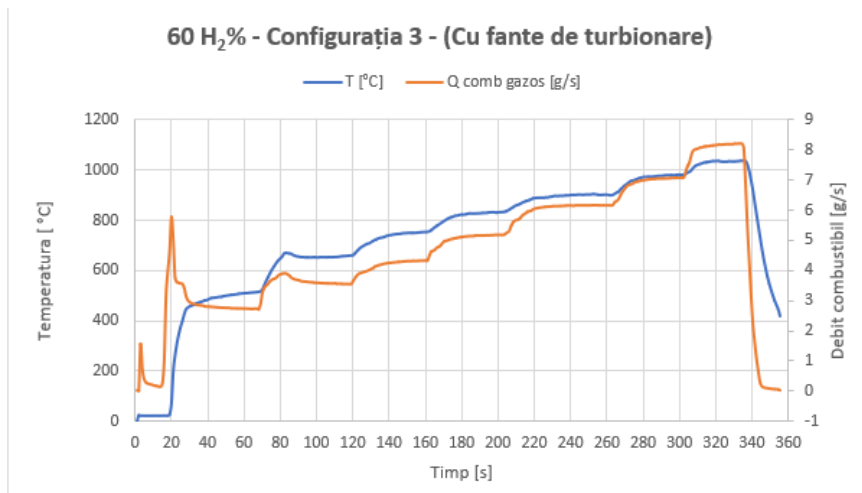


Figure 2.29- Variation during experiments of temperature and fuel flow rate for test configuration 3 at 60%H<sub>2</sub> in mixture

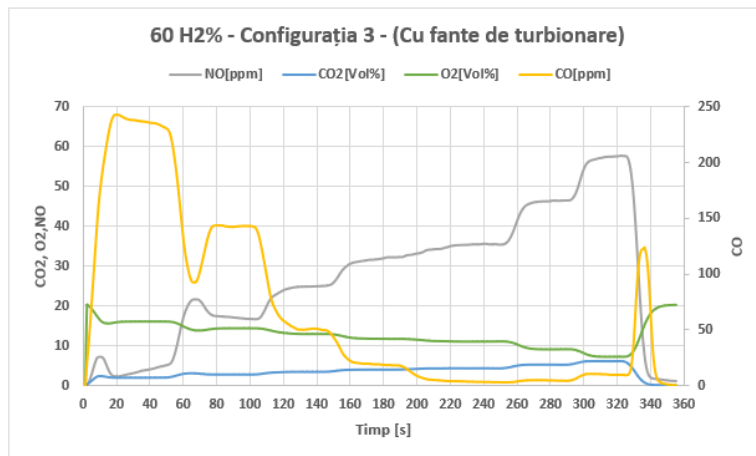


Figure 2.30- Variation during experiments of NO,CO,CO and O<sub>2</sub>, for test configuration number 3 at 60%H<sub>2</sub> in the mixture

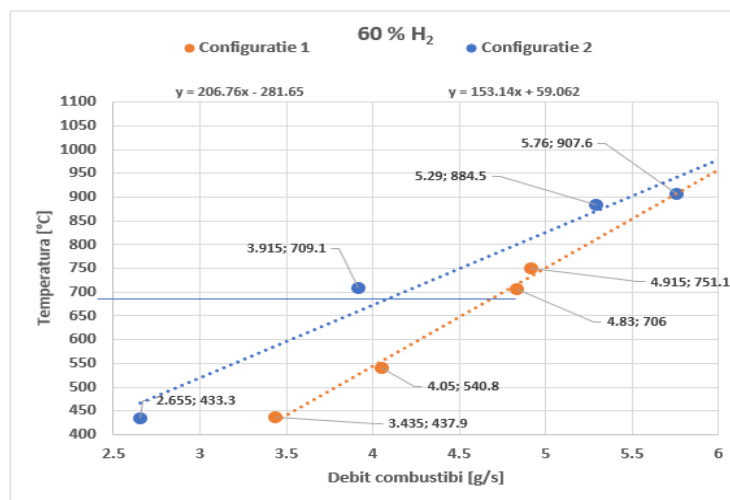


Figure 2.31- Comparison of the temperature evolution for configuration 1 (without copper sieve) and configuration 2 (with copper sieve) at 60% H<sub>2</sub> in the fuel mixture

The variations of flow rate with temperature, in both tested configurations, are linear and directly proportional for an air flow rate of 0.02 kg/s. The use of the copper screen in configuration 2 implies an absolute percentage difference of 26% with respect to configuration 1 in terms of the slope of the graph.

The two graphs for test configurations 1 and 2 have a convergent trend with respect to each other, the point of intersection being reached according to the trend of the captured linear evolution above the maximum test temperature recorded.

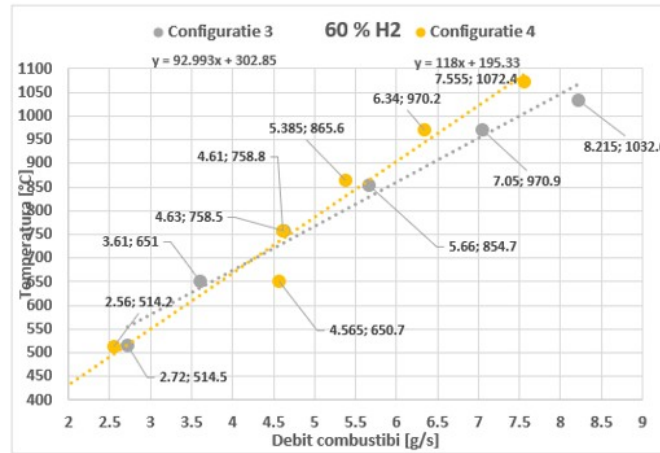


Figure 2.32- Comparison of the temperature evolution for configuration 3 (with swirl nozzles) and configuration 4 (with swirl nozzles and copper sieve) at 60% H<sub>2</sub> in the fuel mixture

The variations of flow rate with temperature, in both configurations tested, are linear and directly proportional for an air flow rate of 0.02 kg/s. The use of the copper screen in configuration 4 implies an absolute percentage difference of 26% with respect to configuration 3 in terms of the slope of the graph.

The two test configurations 2 and 4 have a similar trend with respect to each other, with convergence being reached according to the captured linear evolution trend around the temperature of 750°C. In contrast to configuration 1, where the maximum temperature up to which stand testing was attempted was around 750 °C (due to the noise being too loud), in configuration 3 and 4, the exhaust temperature reached thresholds of 1032 °C and 1072 °C respectively, safe in terms of the initial noise identified. The recorded flow rates are not significantly different for the 2 configurations, thus the differences are only given by the ambient air state parameters.

### 2.4.4.3 Experimental campaign records with 20%CH<sub>4</sub>+80%H<sub>2</sub>

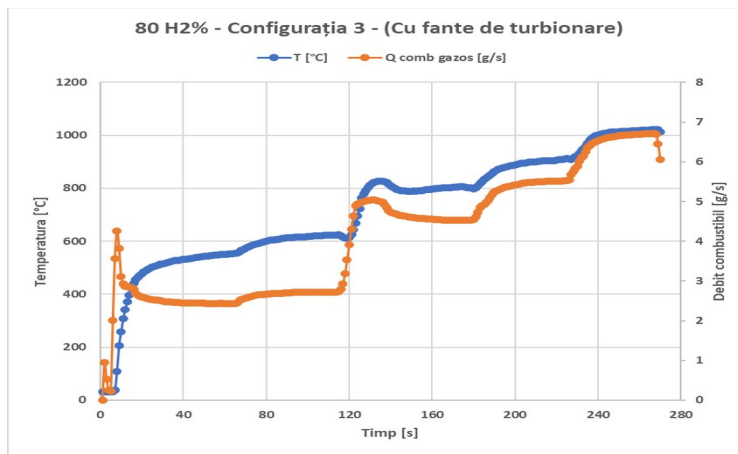


Figure 2.33- Variation during experiments of temperature and fuel flow rate for test configuration 3 at 80%H<sub>2</sub> in mixture

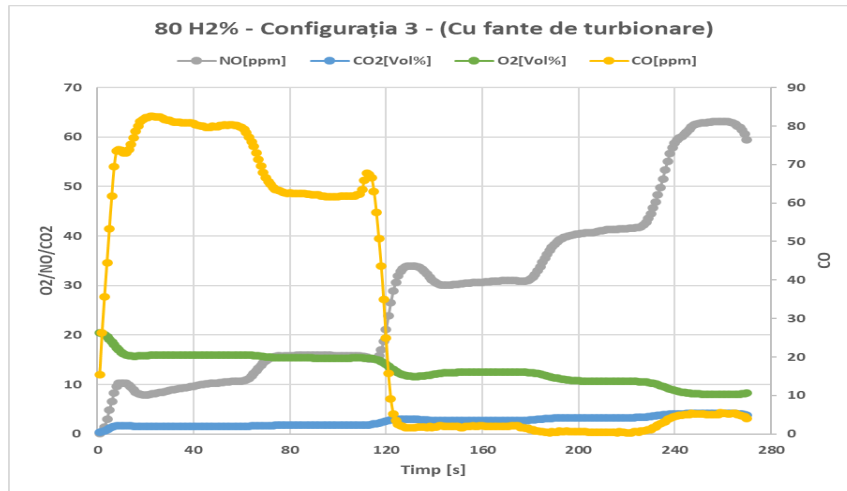


Figure 2.34- Variation during the experiments of NO,CO,CO and O<sub>2</sub>, for test configuration 3 at 80%H<sub>2</sub> in the mixture

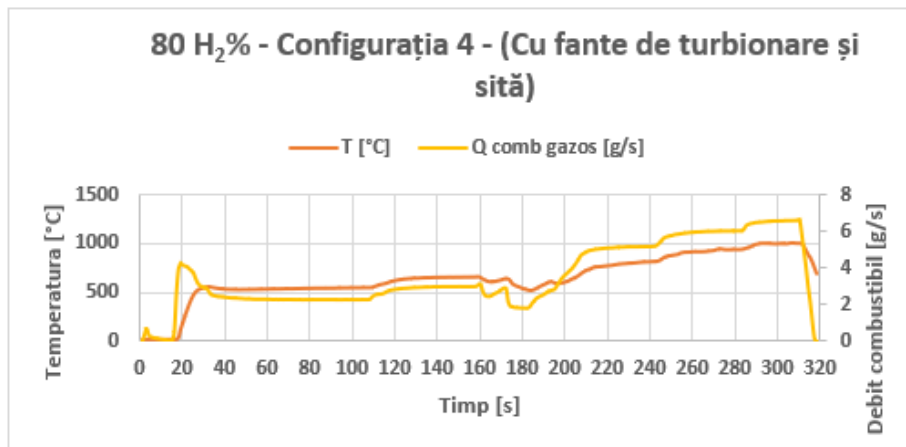


Figure 2.35- Variation during experiments of temperature and fuel flow rate for test configuration 4 at 80%H<sub>2</sub> in mixture

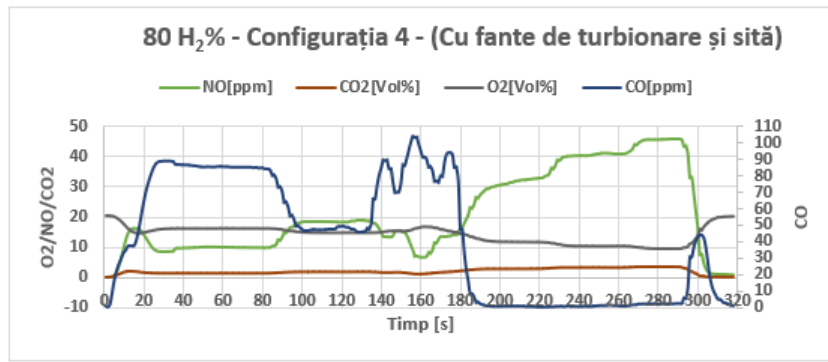


Figure 2.36- Variation during the experiments of NO,CO,CO and O2, for test configuration 4 at 80%H2 in the mixture

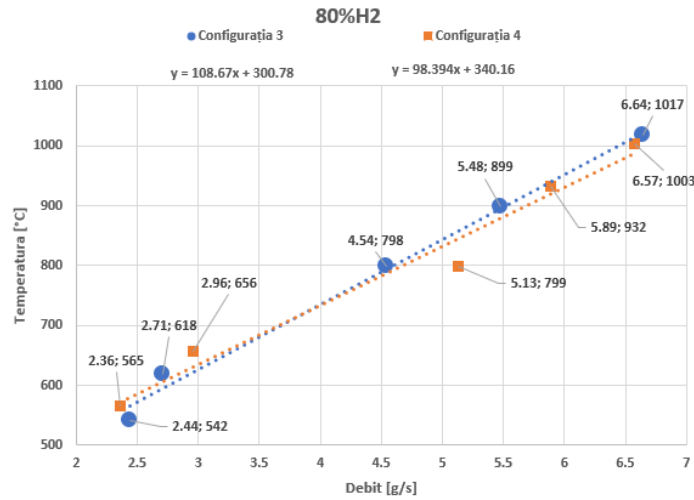


Figure 2.37- Comparison of the temperature evolution for configuration 1 (without copper sieve) and configuration 2 (with copper sieve) at 60% H2 in the fuel mixture

In Figure 2.37 the following can be observed: The variations of flow rate with temperature, in both configurations tested, are linear and directly proportional for an air flow rate of 0.02 kg/s. The use of the copper screen in configuration2 implies an absolute percentage difference of 9.25% with respect to configuration1 in terms of the slope of the graph. No noticeable differences are observed between the two configurations tested in terms of the fuel flow rates used to achieve the temperatures at the measurement point. In Fig. 2.38 the following can be observed: The NO and CO emission trends are similar for both tested configurations with insignificant differences for the same temperature thresholds. Due to the carbon content of the fuel mixture (66% CH<sub>4</sub> by mass) the carbon monoxide emissions have values in the order of tens, expressed in units [ppm], in contrast to the mixtures with 40% respectively 60% H<sub>2</sub> (rest CH<sub>4</sub>).



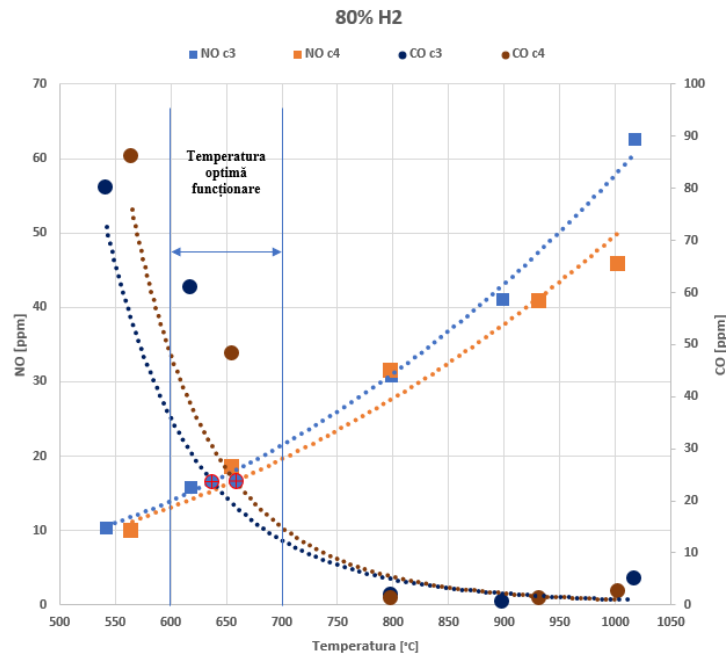


Figure 2.38- Evolution of NO and CO emissions in test setups 3 (with swirl nozzles) and 4 (with swirl nozzles and copper sieve)

#### 2.4.4.4 Experimental campaign records with 100% H<sub>2</sub>:

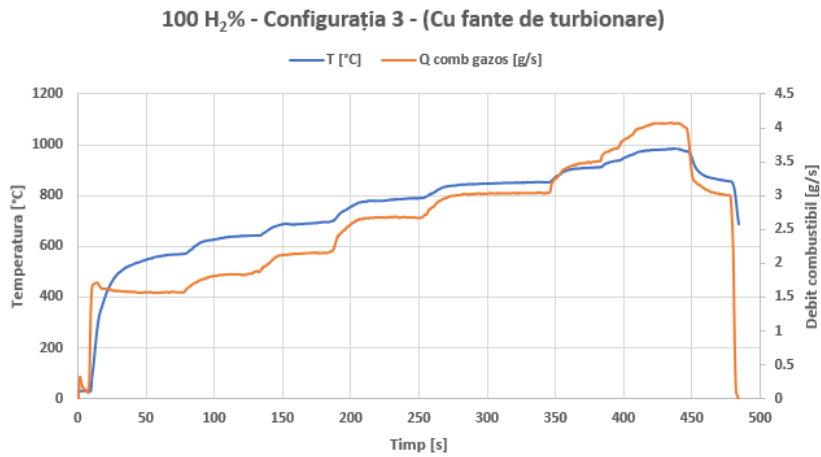


Figure 2.39- Variation during experiments of temperature and fuel flow rate for configuration test number 3 at 100% H<sub>2</sub>

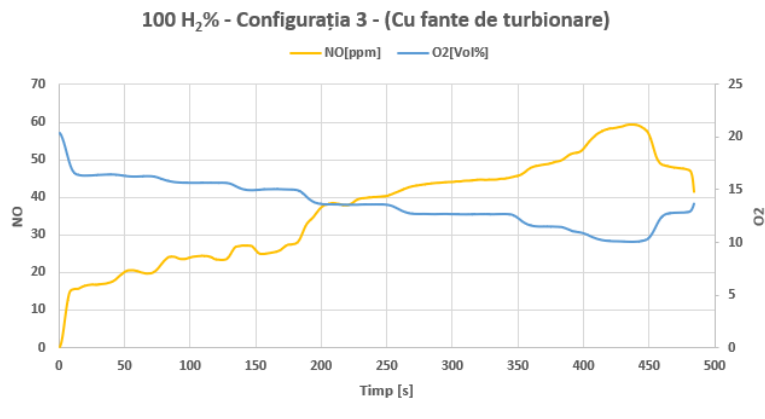


Figure 2.40- Variation during experiments of NO, CO, CO and O2, for test configuration number 3 at 100%H2

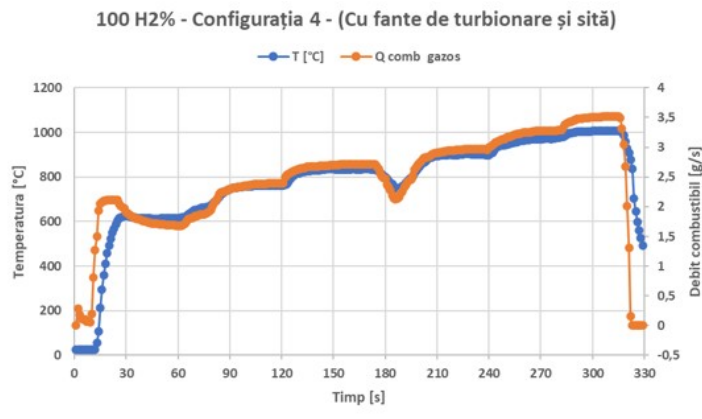


Figure 2.41- Variation during experiments of temperature and fuel flow rate for configuration test number 4 at 100%H2 in mixture

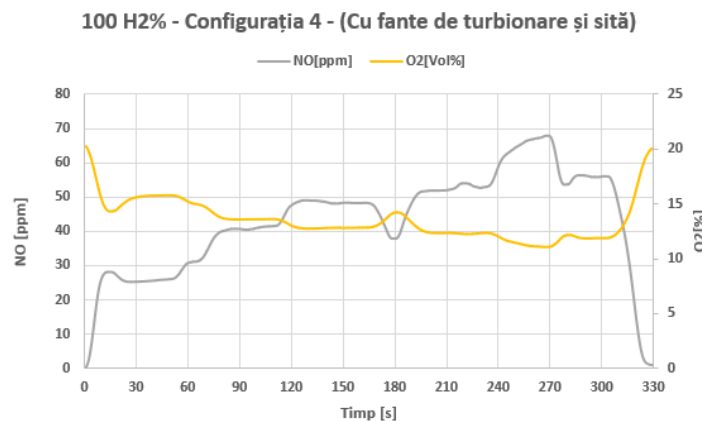


Figure 2.42- Variation during experiments of NO and O2, for test configuration 4 at 100%H2 in mixture

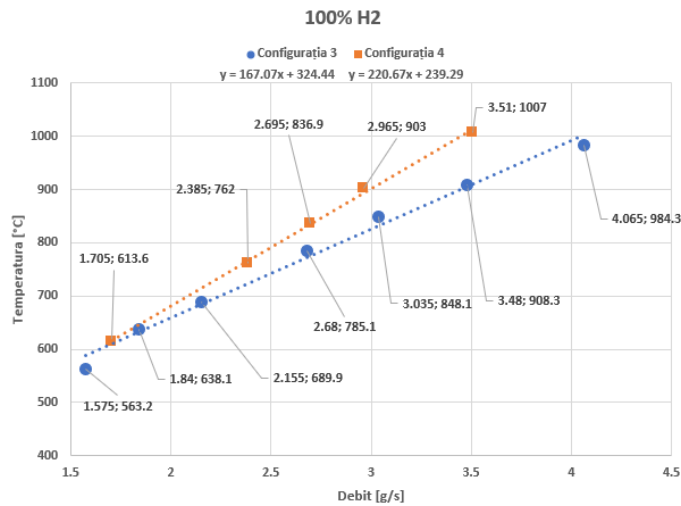


Figure 2.43- Comparison of the temperature evolution for configuration 3 (with swirl nozzles) and configuration 4 (with swirl nozzles and copper sieve) at 100% H<sub>2</sub> in the fuel mixture

In Figure 2.43 the following can be observed: The variations of flow rate with temperature, in both configurations tested, are linear and directly proportional for an air flow rate of 0.02 kg/s. The use of the copper screen, implies an absolute percentage difference of 24% with respect to configuration 1 in terms of the slope of the graph. The differences between the measured temperatures for the same fuel flow rates conveyed are within a range of 50 to 100°C, with a slightly increasing trend in configuration 4.

#### 2.4.4.5 Acoustic determinations on the experimental installation.

In the first stage, the influence of the geometry on the non-reactive flow was identified, for which the noise level emitted by the source at a flow rate of 0.02 kg/s air conveyed through the experimental installation was determined. It is important to note that under no-fire flow conditions in the spectrum of microphone 2 a peak is observed at the frequencies of 317 Hz and 451 Hz which signifies that at these frequencies are excited in turn by several resonant frequencies of the quartz tube (see detail a Fig. 2.44) and of the duct section supplying air to the experimental section (see detail b Fig. 2.44). Because in this case only air flow is involved with low turbulence producing low noise (compared to a reactive flow), these tube resonance frequencies have low amplitudes.

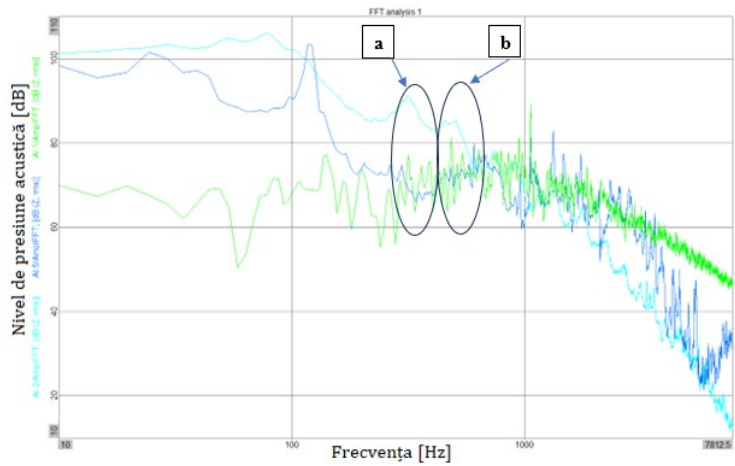


Figure 2.44- Non-reactive flow (air only) with frequency - Hz on the abscissa and sound pressure level - dB on the ordinate

In this case, the speed of sound is considered to be 340 m/s at a temperature of 15°C and for the values of the frequencies presented, respectively:  $f_1=317\text{ Hz}$ ;  $f_2=451\text{ Hz}$ , the result is  $L_1=0,562\text{ m}$ ;  $L_2=0,376\text{ m}$ . This confirms the influence of the quartz tube and the whole test installation as shown in Figure 2.14 in the generation of acoustic pressure waves that will be amplified when temperature gradients appear at the walls in case of fuel combustion in the volume bounded by them.

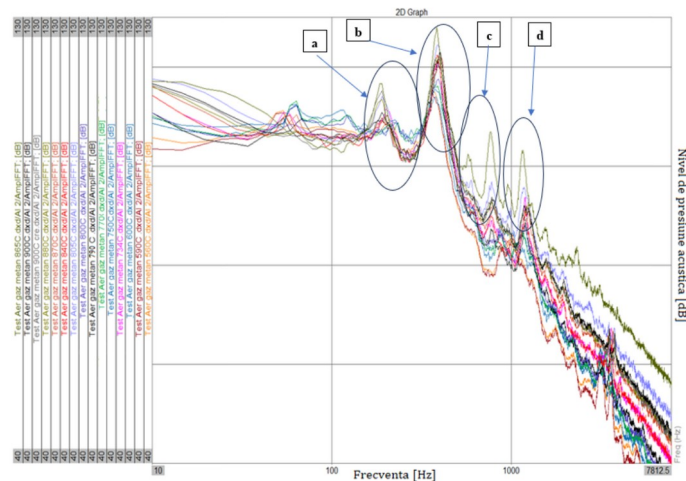


Figure 2.45- Analiza spectrală pentru curgerea reactivă ( $\text{CH}_4$ ) ale datelor înregistrate cu microfonul AI2 pentru conFigureția 1 de testare

The following can be observed in Fig. 2.45: The appearance of a spectral component at 190 Hz only at high temperatures ( $>800^\circ\text{C}$ ) which is in fact the fundamental frequency - (see a). The same spectral component appears at 385 Hz which is the 1st harmonic and has higher amplitudes in the reactive flow ( $\text{CH}_4$  burning) situation - (see b), This component has 2nd and 3rd harmonics at 524 Hz and 771 Hz respectively, temperature leads to increase in amplitude - (see c). The 4th harmonic corresponds to a frequency of 1166 Hz, above this value the harmonics

are no longer of interest - (see d). In Fig. 2.46, which is shown below the acoustic spectra for the combustion of a mixture of 80% CH<sub>4</sub> enriched with 20% H<sub>2</sub> at different operating temperature regimes are compared. Separately, the acoustic spectra for the combustion of the mixtures 60% CH<sub>4</sub> enriched with 40% H<sub>2</sub>, respectively 40% CH<sub>4</sub> enriched with 60% H<sub>2</sub> are presented in Figure 2.47. Based on the case analysis Fig. 2.46 the following aspects have been observed: Burning a mixture with 20% H<sub>2</sub> leads to the generation of a strong tone with fundamental frequency between 209-239 Hz - (see a), The first harmonic of this spectrum appears at 412 Hz - (see b), The second harmonic and the third harmonic appear at 512 Hz, respectively 625 Hz - (see c),

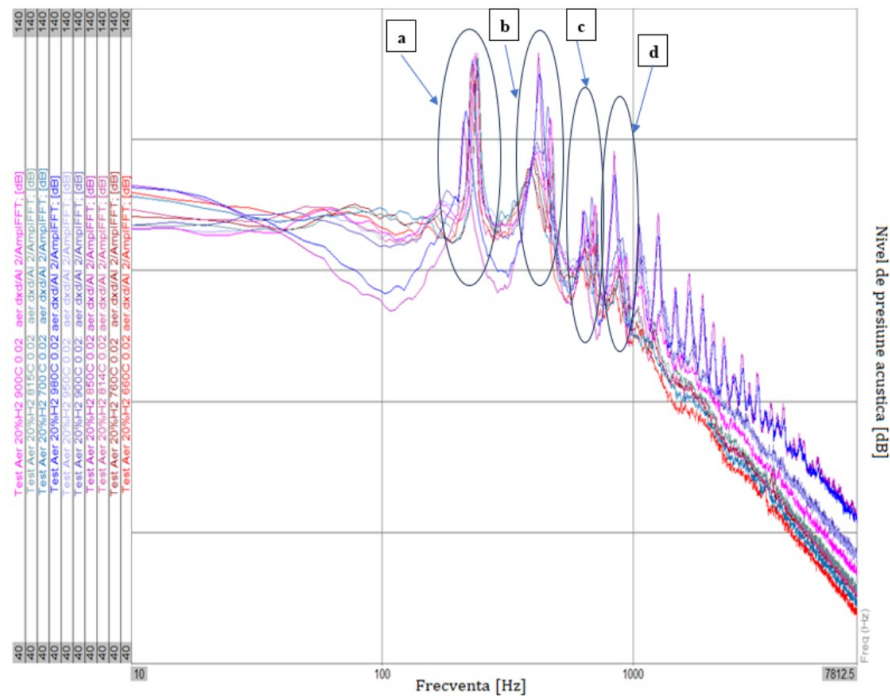


Figure 2.46-. Spectral analysis for the reactive flow (80%CH<sub>4</sub>+20%H<sub>2</sub>) of the data recorded with the AI2 microphone for the test configuration 1

Based on the analysis of Fig. 2.47 the following aspects were noted: As the volume concentration of H<sub>2</sub> increased, the spectrum was strongly altered. The burning of mixtures with 40% respectively 60% H<sub>2</sub> (volumic) leads to the generation of strong tones with fundamental frequencies ranging from 288-361 Hz the rest being harmonics - (see a). The peaks of the spectrum plots for the frequencies related to 1st (b), 2nd and 3rd(c), 4th(d) order harmonics have different amplitudes from those observed in the spectral analysis shown in Fig. 2.63. The appearance of these identified harmonics at higher frequencies did not lead to a direct and clear link as to why variation in hydrogen content in the mixture (but also temperature) alters the frequency variation, but the observed trend is that the pitch fundamental increases in frequency with varying concentration and temperature.

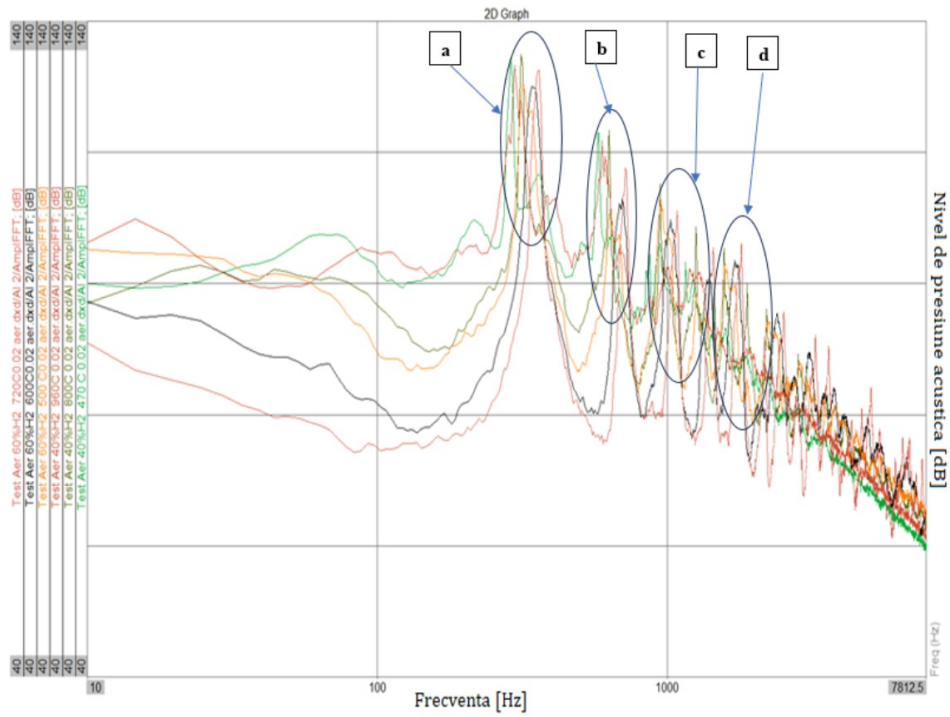


Figure 2.47- Spectral analysis for the reactive flow (60%CH<sub>4</sub>+40%H<sub>2</sub> respectively 40%CH<sub>4</sub>+60%H<sub>2</sub>) of the data recorded with the AI2 microphone for the test configuration 1

#### 2.4.4.6 Acoustic determinations in the situation of gas combustion of hydrogen-enriched methane gas mixtures on the experimental test rig

Due to the very loud noise measured by microphones 2 and 5, the dynamic measuring range of the microphones was exceeded and the system overloaded. Thus, the peaks of the signals picked up by microphones 2 and 5 are truncated and the frequency analysis will indicate lower amplitudes on the spectral components than those perceived in reality. To observe this phenomenon, the following image shows the waveform of an acoustic signal that has not exceeded the dynamic range and the waveform of a signal that has overloaded.

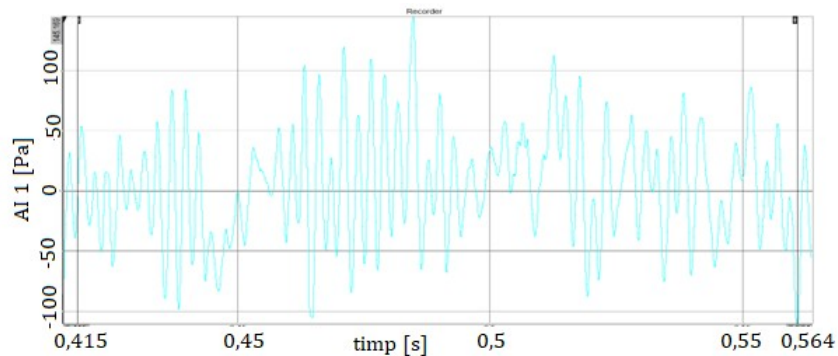


Figure 2.48- Example of a correct signal

Table 2.3 Experimental data for acoustic analysis c1 and c2

Configurația 1 Configurația 2	Roșu Albăstru	Temperatura	Temperatura medie	Microfon AII		
				Fundamentala		Valoarea integrată
X% H <sub>2</sub>	Plot	[°C]	[°C]	Frecvențe [Hz]	Amplitudini [dB]	RMS [dB]
20	Plot 1	660	I 680	229	109,372	121
		700		229	94	115
	Plot 2	814	II 822	229	110	124
		830		224	93	117,4
	Plot 3	950	III 960	229	114	128,4
		970		209	95	118,7
40	Plot 4	470	I 470	288	123	137,2
		470		273	122	134,5
	Plot 5	800	II 800	312	124	135
		800		273	119	131,9
	Plot 6	960	III 955	297	123	136
		950		263	110	124
60	Plot 7	500	I 465	317	125	142
		430		292	128	139
	Plot 8	600	II 650	341	129	146
		700		322	131	141
	Plot 9	720	III 767,5	361	132	144
		815		332	129	140

Note the integrated sound pressure values recorded when burning a 40%CH<sub>4</sub>-60%H<sub>2</sub> mixture in configuration 1 of the test. The noise produced, comparable to the take-off of an airplane, exceeded at about 1 meter from the source the value of 140 dB, which has destructive potential for both the plant and the operator.

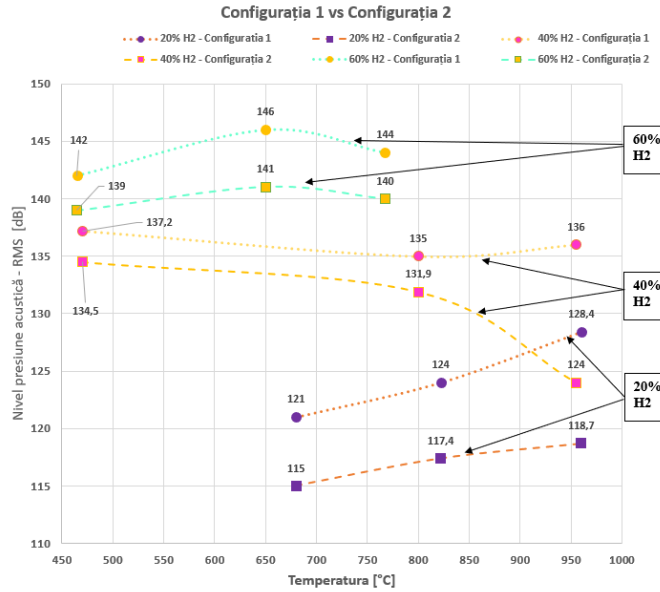


Figure 2.49- Comparison of sound pressure levels recorded for configuration 1 (dashed line) and configuration 2 (dashed thick line) for burning mixtures with 20%, 40% and 60% H<sub>2</sub> in the composition

In Figure 2.49 it can be seen that for each tested composition, the use of the copper screen upstream of the swirler, namely the solution tested in configuration 2, achieved the attenuation of the acoustic pressure level in favor of its use and the results are as shown in the Table :

**Table 2.4 Noise level comparison between c1 and c2**

X%H <sub>2</sub>	Diferența medie a nivelului de zgomot C2 față de C1 [dB]	Diferență procentuală a reducerii zgomotului pe fiecare regim de temperaturi testat [%]	
		I	II
20	-7,4	I	5,22
		II	5,62
		III	8,17
40	-5,9	I	2,01
		II	2,35
		III	9,68
60	-4	I	2,16
		II	3,55
		III	2,86

In this previously presented comparison, it was found that the copper screen reduced the noise in all operating regimes (I, II, III), mitigating the effects of the thermoacoustic phenomenon encountered in the situation of combustion of CH<sub>4</sub>-H<sub>2</sub> mixtures on the test stand. The fact that the sound intensity reduction values are between 4-8 dB denotes that the changes are notable and sufficiently important in operation, taking into account that the variation from the initial value of the sound pressure level to its value after using the copper screen. In this comparison, between test configuration 3 and 4 respectively, lower values of the sound pressure level are noted compared to the values measured in the comparison between test configuration 1 and 2 respectively. Here a maximum value of 128.7 dB is identified, by much lower than the maximum values identified in previous test sessions. In Fig. 2.50 it is observed that in the case of mixtures of 60% H<sub>2</sub> in the mixture, the copper screen contributes very little in terms of noise attenuation, but at all operating modes it brings a decrease in the recorded sound pressure level.



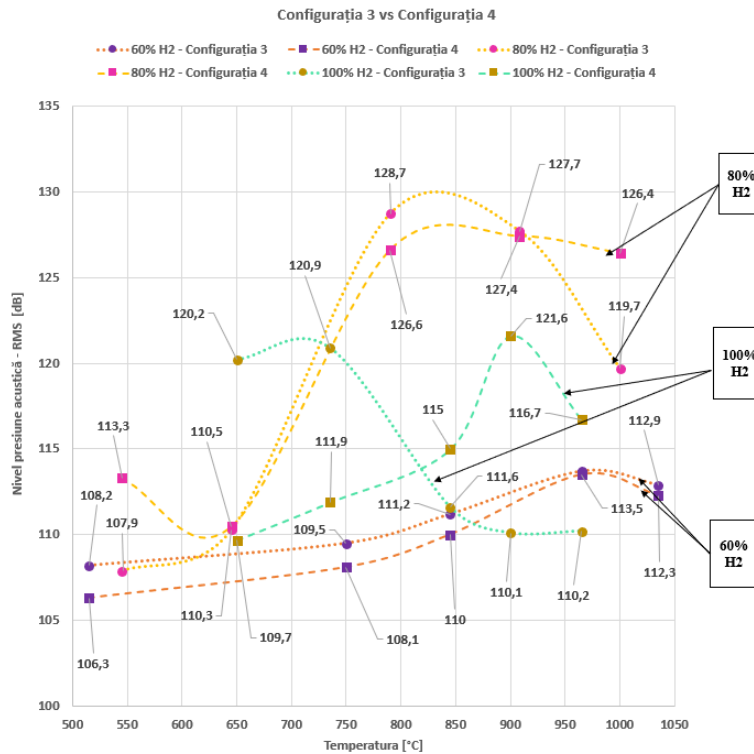


Figure 2.50- Comparison of sound pressure levels recorded for test configurations 3 (dotted line) and 4 (dashed line) when burning mixtures with 60%, 80% and 100% H<sub>2</sub> in composition

## 2.5 Experimental campaign (conclusions)

Experimental results show that the combustion of methane and hydrogen mixtures involves complex challenges related to noise, flame stability and gas emissions. Hydrogen, due to its fast-burning properties, introduces a more intense acoustic behavior and large temperature fluctuations, especially at high concentrations. The proposed technical solutions, such as porous copper discs and changes in the geometry of the combustion chamber, had a positive impact on reducing noise and improving combustion stability. The introduction of copper screens has reduced noise levels by up to 8 dB in certain configurations, making these solutions viable for industrial applications where safety and energy efficiency are critical.

**Configuration 1: No copper screen.** This was the first basic configuration, where air and fuel were injected into the combustion chamber through a classic swirler. The noise generated in this configuration was significant, especially at high temperatures and in mixtures with a high hydrogen content. **Configuration 2: With copper screen.** In this configuration, a porous copper disc was inserted in front of the swirler to reduce noise and even out the air flow. This solution resulted in a significant reduction in noise and more stable combustion in hydrogen-rich mixtures. **Configuration 3: With swirl slots.** The third configuration involved changing the

geometry of the combustion chamber by adding slots to optimize airflow and improve the air-fuel mixture. This modification allowed the hydrogen concentration in the mixture to increase to 100% H<sub>2</sub> without producing excessive noise. **Configuration 4: With swirl slots and copper screen**. This combined the solutions of configurations 2 and 3, including both copper discs and swirl slots. Configuration 4 also demonstrated good results in terms of combustion stability and control of acoustic phenomena. However, future research directions include further optimization of these solutions and extension of the study to other types of hydrogen-enriched fuels. It is also desired to develop methods to further mitigate noise and emissions by using new materials, such as metal foams or ceramic resins, which can dissipate acoustic energy more efficiently and withstand high temperatures.

### 3. Numerical modeling of reactive turbulent flow

#### 3.1 Introduction

Fluid flow is governed by a set of equations known as the Navier-Stokes equations. This system of equations with partial derivatives is based on fundamental laws of conservation of mass, momentum, energy and chemical species. Thus an analytical solution of this system of equations would provide an exact description of the flow of a reactive fluid.

In turbulent flows, the inertial forces exceed the viscous forces in magnitude, so that the instabilities developing in the flow tend to grow and rapidly form large rotating structures characterized by the integral length scale,  $l_0$ . These large rotating structures are subjected to stretching and break into smaller and smaller structures, until the so-called Kolmogorov limit is reached. If  $l_0$  is comparable to the largest length scales involved in the flow and is in a domain where computational grids of reasonable resolution can capture it, then the Kolmogorov length scale is much smaller and a numerical integration to capture this scale becomes impractical from the point of view of computing resources. Such an approach, to solve all length scales down to the smallest (Kolmogorov scale), is known in the literature as DNS. The Reynolds number up to which the DNS method can be used is around 6000 [9]. A first solution to the problem of computational resources raised by turbulent flows is the so-called "Reynolds averaging of the Navier-Stokes equations" (RANS) technique. In the RANS method, the Navier-Stokes equations are averaged over time. Only the time-averaged flow field has to be solved in this way, thus eliminating the temporal fluctuations due to the small scales involved in the turbulent motion,

and allowing the use of much coarser discretization grids and requiring significantly reduced computational resources.

### 3.2 Elements of the kinetics of chemical reactions

The burning process is the result of a strongly exothermic chemical reaction, the result of energy exchanges that occur together with intermolecular collisions. In general, at ordinary temperatures, a chemical reaction occurs very slowly, because the molecules, although they collide, cannot play a sufficient amount of energy to carry out the chemical transformation.

If the reaction speed is defined  $\bar{w} \left[ \frac{\text{molecule}}{m^3 s} \right]$ , as the number of molecules transformed in the unit of time and in the unit of volume, it will be proportional, according to the hypothesis of collision reactions, with the number of molecules of active substances, namely with their concentrations:

$$\bar{w} = k \cdot C_1 \cdot C_2 \cdot C_3 \dots \quad (3.1)$$

where the coefficient  $k$  expresses the fact that only a part of the collisions are effective. According to the theory of chemical kinetics, only "active" collisions lead to the chemical reaction, that is, collisions involving molecules with an initial energy greater than or equal to a

determined energy, which is noted  $E_a \left( \frac{J}{kmol} \right)$  and which is called activation energy. This energy is necessary to destroy or weaken existing intramolecular bonds [60].

#### 3.2.1 Mechanism of the CH<sub>4</sub>/air reaction

In the present study, a two-step reaction mechanism was used for the numerical modeling of the CH<sub>4</sub>/air combustion process. The reaction mechanism is described by the following chemical equations:



#### 3.2.2 H<sub>2</sub>/air reaction mechanism

The main chain of hydrogen combustion reactions is represented in Figure 3.1, where the major reaction pathways are highlighted. These pathways were selected based on the specific rate of each elementary reaction. Thus, the emphasis is placed on the reactions with the highest rate, with the result that the slower reactions, which are determined by the reaction rate constant, become dominant in controlling the entire combustion process. This approach provides a detailed

assessment of hydrogen combustion mechanisms, providing essential information for numerical simulation and process optimization in various experimental and industrial scenarios.

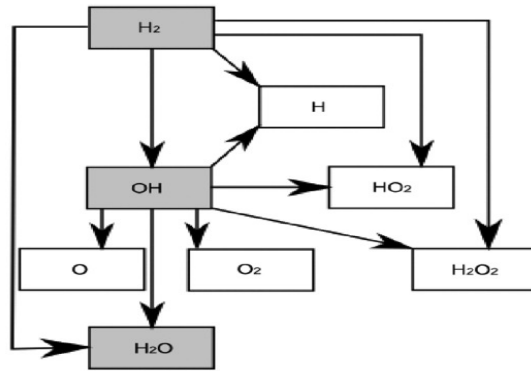


Figure 3.1 Main chain diagram for the reduced oxidation reaction mechanism of hydrogen

The reaction mechanism reduction strategy is based on stationary process and partial equilibrium assumptions. In the case of a homogeneous system, the steady state assumption is applicable for those intermediate species that are produced by slow reactions and consumed by fast reactions, so that their concentration is kept low. The assumption of partial equilibrium can be justified when the reaction rate coefficients for reversible reactions are significantly higher than those of all other reactions [10]. Table 3.1 shows the H<sub>2</sub>/air reaction mechanism used in the numerical simulations.

**Table 3.1** Hydrogen oxidation mechanism [11]

Nr	Reactanți		Prođuși	A	n	Ea kJ/g*mol	Ea j/kg- mol
1	H+O <sub>2</sub>	→	OH+O	1,20E+17	-0,91	69,1	6,91E+07
2	OH+O	→	O <sub>2</sub> +H	1,80E+13	0	0	0
3	O+H <sub>2</sub>	→	OH+H	1,50E+07	2	31,6	3,16E+07
4	OH+H <sub>2</sub>	→	H <sub>2</sub> O+H	1,50E+08	1,6	13,8	1,38E+07
5	H+H <sub>2</sub> O	→	OH+H <sub>2</sub>	4,60E+08	1,6	77,7	7,77E+07
6	O+H <sub>2</sub> O	→	OH+OH	1,50E+10	1,14	72,2	7,22E+07
7	H+H+M(H <sub>2</sub> )	→	H <sub>2</sub> +M(H <sub>2</sub> )	7,00E+15	-0,6	0	0,00E+00
8	H <sub>2</sub> +M(H <sub>2</sub> )	→	H+H+M(H <sub>2</sub> )	8,80E+14	0	402	4,02E+08
9	H+OH+M(H <sub>2</sub> O)	→	H <sub>2</sub> O+M(H <sub>2</sub> O)	1,40E+23	-2	0	0,00E+00
10	H <sub>2</sub> O+M(H <sub>2</sub> O)	→	H+OH+M(H <sub>2</sub> O)	1,60E+17	0	478	4,78E+08

### 3.3 Numerical modeling for the new swirler for CH<sub>4</sub>/H<sub>2</sub> mixture operation

In this study, RANS-type numerical simulations were carried out using the commercial ANSYS FLUENT software.

#### 3.4.1 Geometry and computational grid

The geometry of the computational domain was made using the 3D Solid Edge design software, based on the configuration of the test stand, which is presented in Figure 3.3. The

computational domain includes the metal cone that represents the front of the burner, the swirl injector, the air path and fuel ports of the burner, and the outer casing.

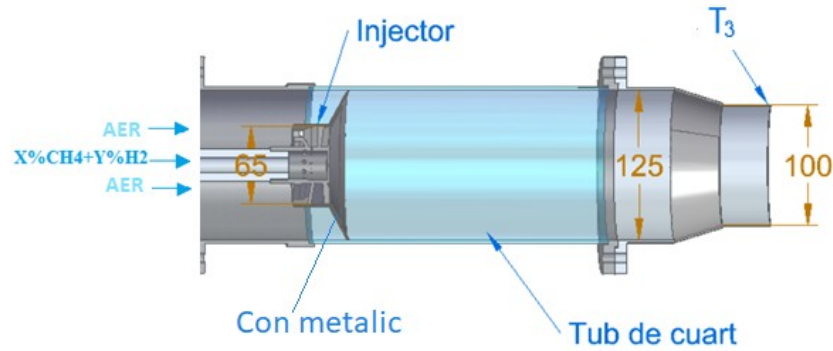


Figure 3.3 3D model of the experimental section

The computational grid consists of an unstructured element mesh generated using ICEM-CFD from the ANSYS package. The network has 6,233,848 elements and 1,056,870 nodes. This was refined inside the fire tube, in the primary zone, as can be seen in Figure 3.2. This density of volume elements has the role of capturing phenomena such as: mixing, the development of recirculation zones as well as the temperature field resulting from the oxidation reaction of fuel mixtures.

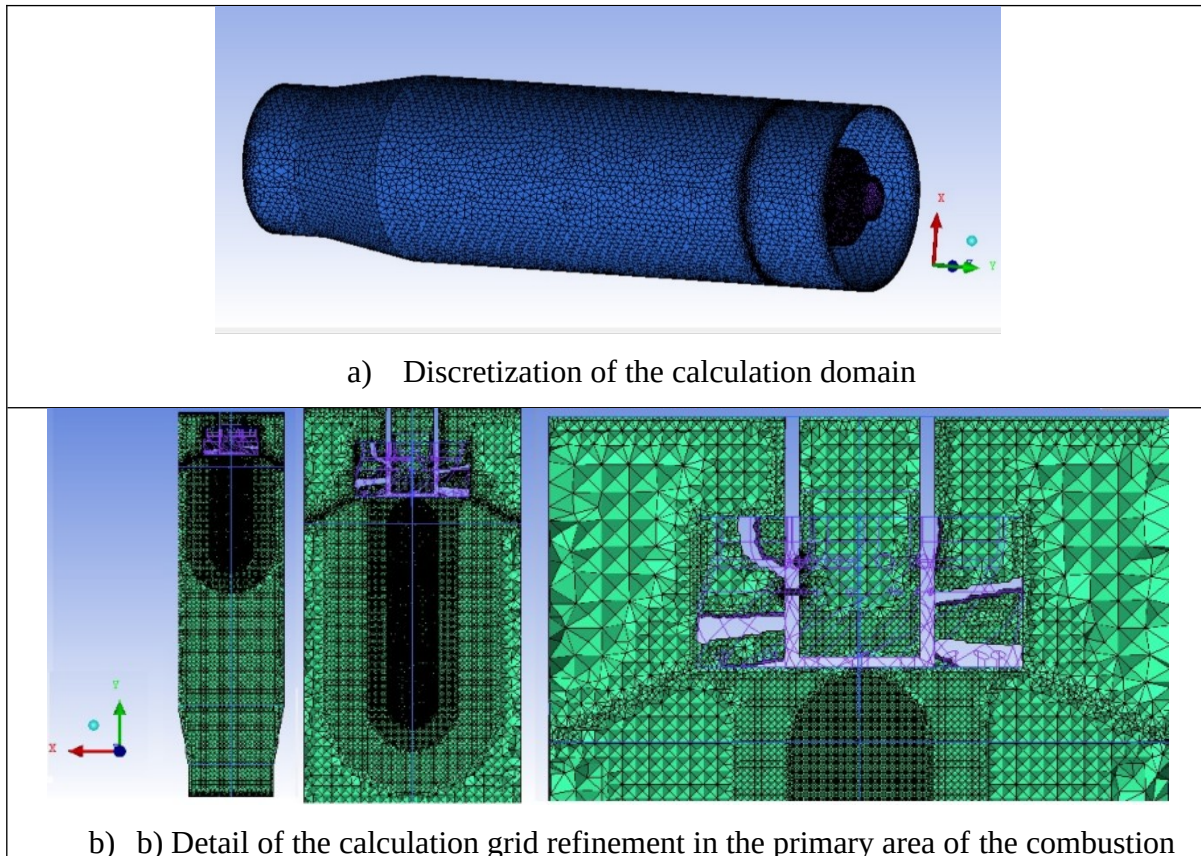


Figure 3.2 Computational grid

### 3.4.2 Boundary conditions

The turbulence model used was of the RANS type, namely the  $k-\epsilon$  model that provides the best results so far in similar cases [12-13]. These fine structures occupy a very small fraction of the actual fluid volume, composed of a two-step methane-air reaction mechanism imported from the ANSYS library and the 10-step reaction mechanism for the hydrogen-air reaction.

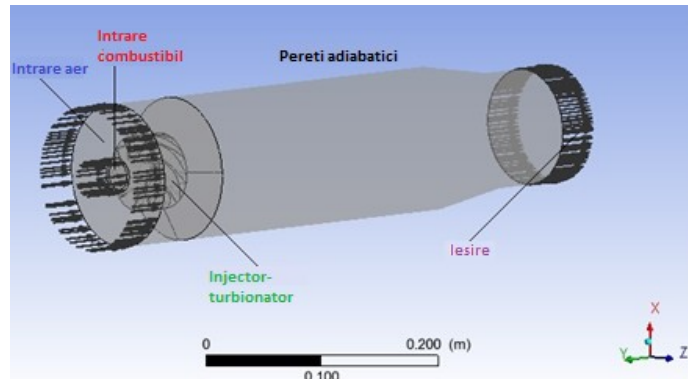


Figure 3.3 Computational domain

The flow rates of the methane-hydrogen mixtures were varied in order to reach at the burner outlet the temperature in relation to the thermal power of 25.5 kW; 19.5 kW and 14.5 kW.

### Numerical modeling results

In the first stage of the study, a comparison was made between two variants of the swirl injector. Both feature radial holes between the swirler blades through which the fuel mixture is injected and partially premixed with air. In the case of the second variant of the injector-turbulent, a hole was added on the front face of the swirler to print a jet in the axial direction in the fire tube. This orifice (2 mm diameter) allows the fuel mixture to be injected into the primary zone resulting in a diffusion flame. The two geometries related to case 1 and case 2 are shown in Fig. 3.4.

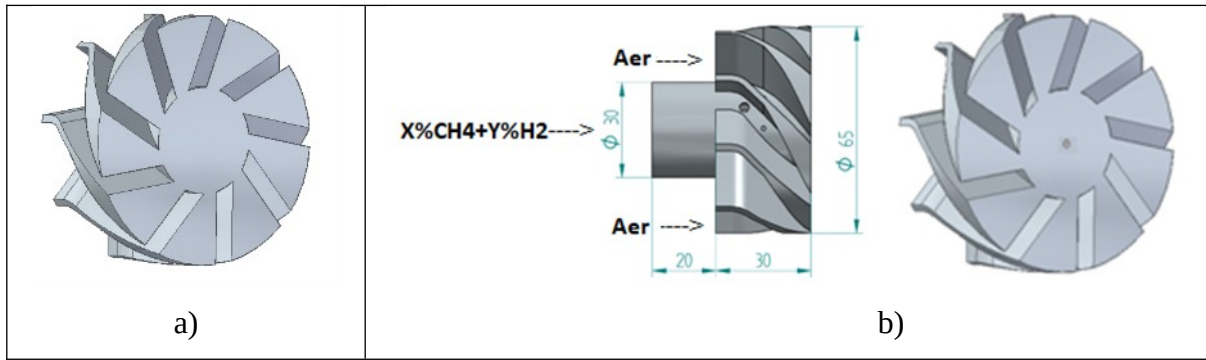


Figure 3.4 The swirl injector a) case 1 and b) case 2

The total average temperature along the burner was monitored to better understand the phenomenon that occurs inside the fire tube during the combustion of hydrogen-enriched methane for each case (Figure 3.5).

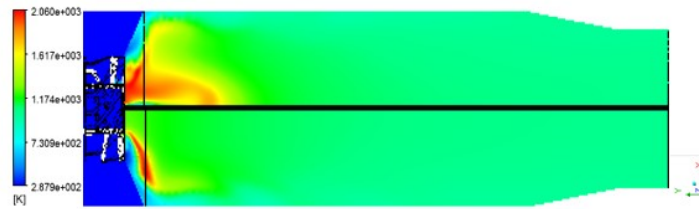


Figure 3.5 Temperature distribution along the combustion chamber (case 1, shown below the black line and case 2 shown above the black line)

Figures 3.6-3.8 show the evolution of temperatures along the combustion chamber. With the solid line are the related graphs for case 1 and with the dotted line for case 2.

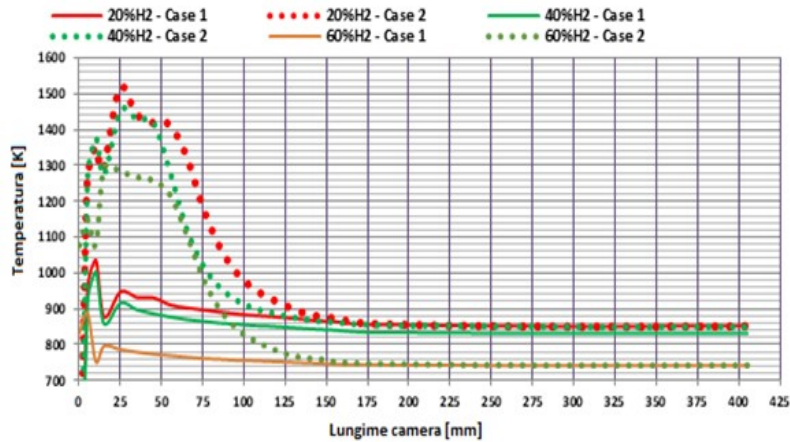


Figure 3.6  $P(t) \approx 14 \text{ kW}$  Air flow = 0.02 kg/s

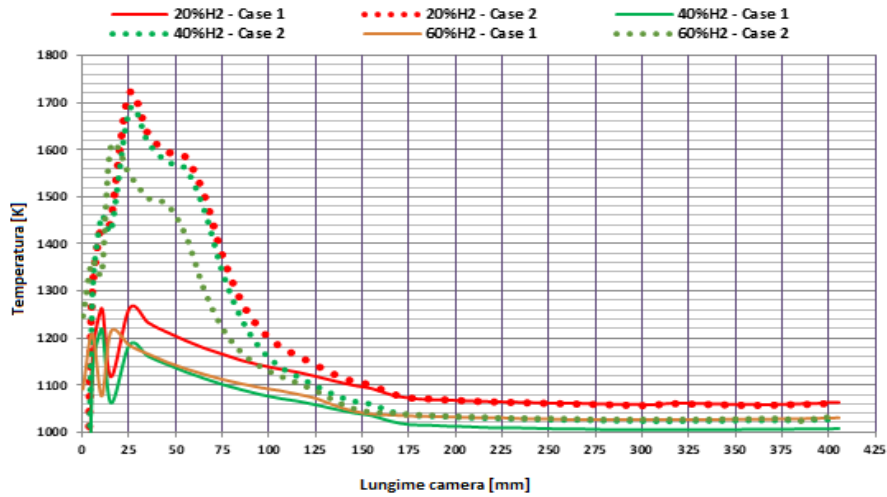


Figure 3.7  $P(t) \approx 19 \text{ kW}$  Air flow = 0.02 kg/s

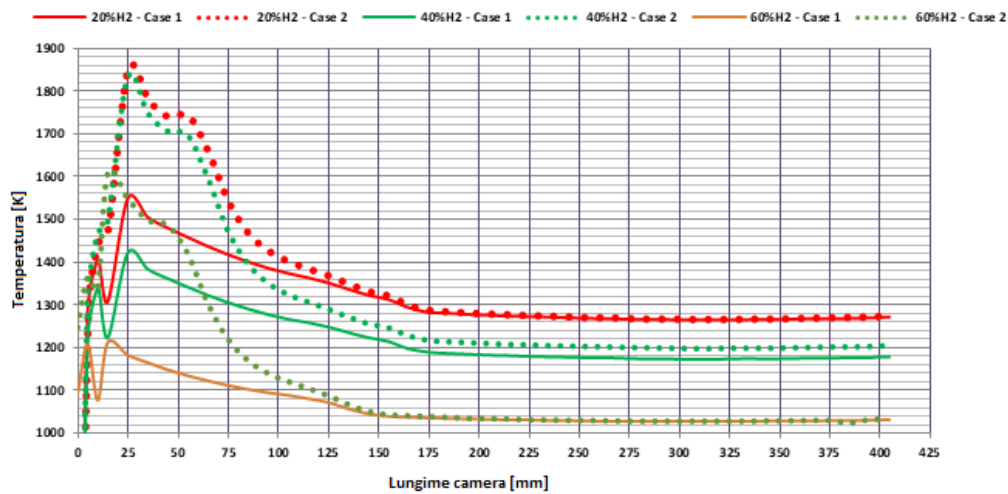


Figure 3.8  $P(t) \approx 24 \text{ kW}$  Air flow = 0.02 kg/s

The velocity vectors are presented in Figure 3.9 for both cases, the highest magnitude being indicated at the exit from the channels for the passage of air between the swirler blades. For case 1, the radial distribution flame (partially premixed) is more extended toward the wall than that shown in case 2 due to the additional fuel flow through the 2 mm diameter front orifice and the velocity reduction through the radial fuel orifices. This resulted in low temperatures near the combustion chamber wall without additional air to provide cooling.



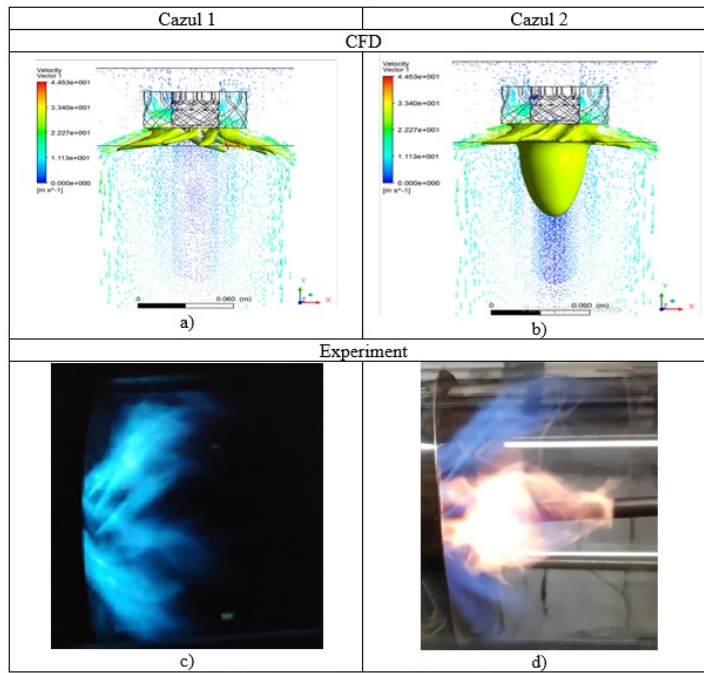


Figure 3.9 CFD flame shape comparison versus Experiment

The results indicated that for the same fuel mass flow, the temperature in the primary zone of the burner in the two cases varied between 200 and 400 K. In case 2, the diffusive flame induced a temperature increase in the first 100 mm of the combustion chamber. Combustion which can lead to the formation of NO<sub>x</sub>. Furthermore, the diffusive flame moved the flame front further away from the swirler injector and the metal cone, and as a result, this will extend the life of the metal parts of the burner. Both in the case of reactive flow as well as in the non-reactive one (only air) through the fire tube, it was found both numerically and experimentally that in its center the direction of the currents is in the opposite direction to the swirling flow, namely from the exit plane from the fire tube to the swirl injector. The center line is shown in Figure 3.10.

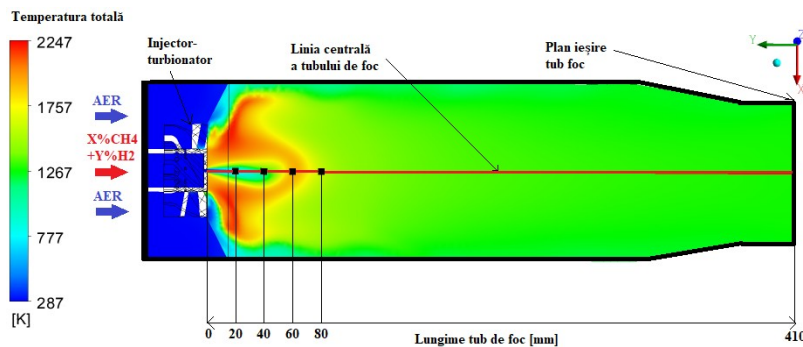


Figure 3.10 Longitudinal section of the computational domain highlighting the centerline of the fire tube and points of interest for velocity measurement in the primary zone

A second variant of the swirl injector developing both the partial premixed flame and the diffusive flame was considered. In order to investigate the chosen reaction mechanism, investigations were carried out in the field of calculation regarding the total temperature, the

speed and direction of the flow, the distribution of the chemical species participating in the combustion reactions. Chemical species were expressed as mass fraction. This is a way of expressing the composition of a component in a mixture or solution, being the ratio between the mass of the component and the total mass in the solution. The fuel considered was 40%CH<sub>4</sub>+60%H<sub>2</sub>.

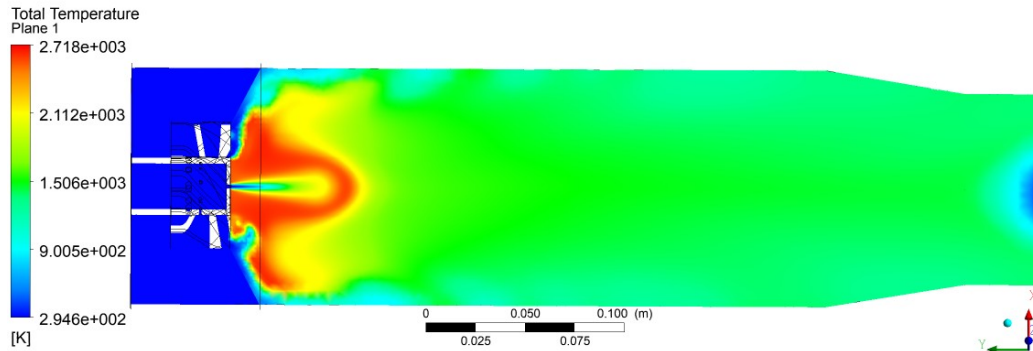


Fig. 3.18 The total temperature in the section of the calculation domain

From Figure 3.11 it can be seen that the high temperature area is found in the primary area of the fire tube. This is desirable for the correct operation of a combustion chamber.

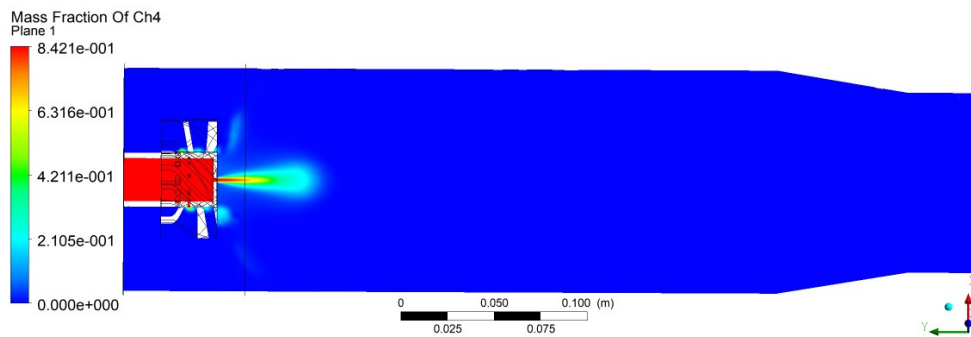


Fig. 3.12 The mass fraction of CH<sub>4</sub> in the section of the calculation domain

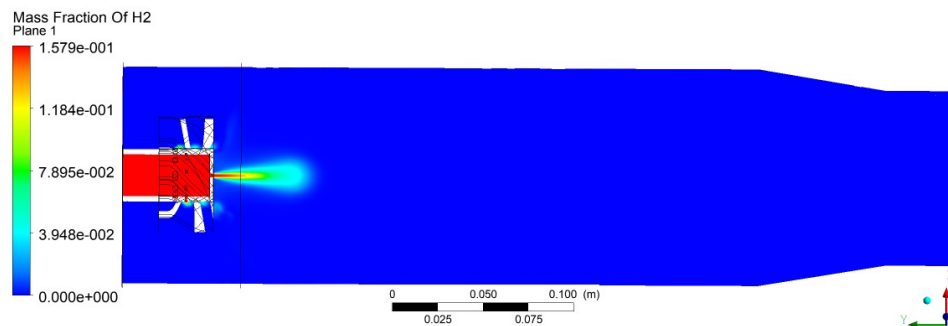


Fig. 3.13 The mass fraction of H<sub>2</sub> in the computational domain section

From Figures 3.12 – 3.13 it can be seen that the fuel mixture is consumed entirely in the primary zone of the fire tube, the mass fractions of H<sub>2</sub> and CH<sub>4</sub> at the exit from the combustion chamber being 0. The reaction products, resulting from the numerical modeling of

the process of combustion, having a significant mass fraction ( $> 10^{-3}$ ), are presented in Figures 3.14-3.16. These reaction products are  $H_2O$ ,  $CO$ , and  $OH$ , respectively.

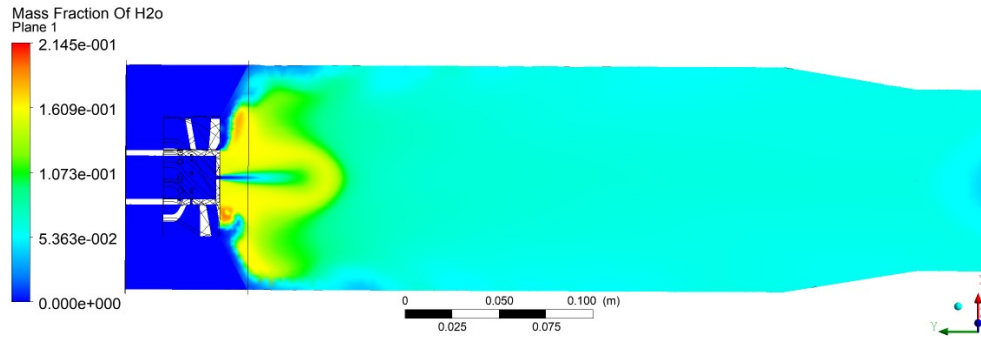


Fig. 3.14 The mass fraction of  $H_2O$  in the computational domain section

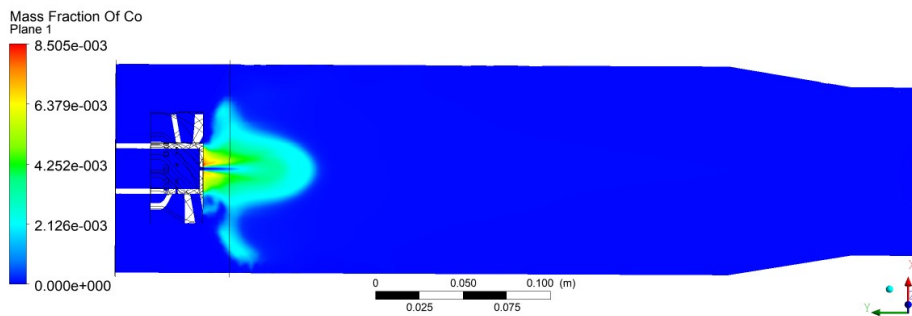


Fig. 3.15 The mass fraction of  $CO$  in the computational domain section

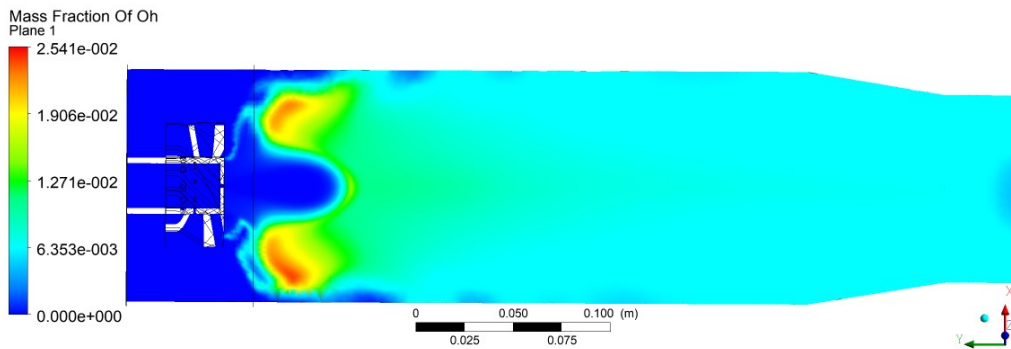


Fig. 3.16 The mass fraction of  $OH$  in the computational domain section

To investigate the area of interest, where the combustion reactions take place, the evolutions of different relevant parameters were monitored in 1000 points along the yellow lines in Fig 3.17. The diameter of the fire tube is 125 mm.

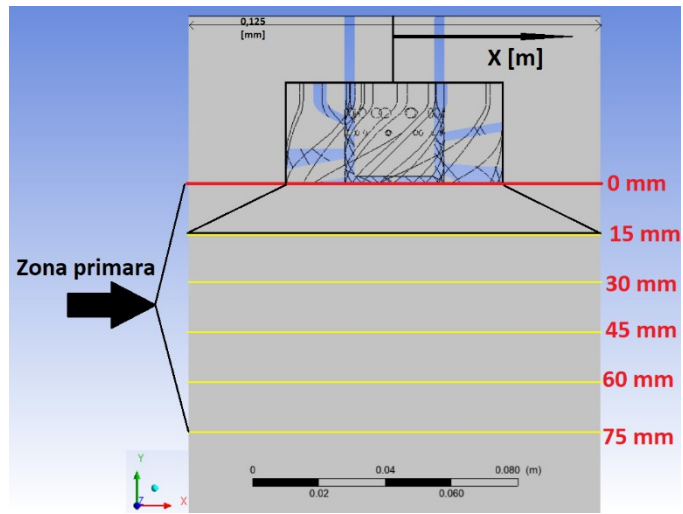


Figure 3.17 Positioning lines for monitoring parameters

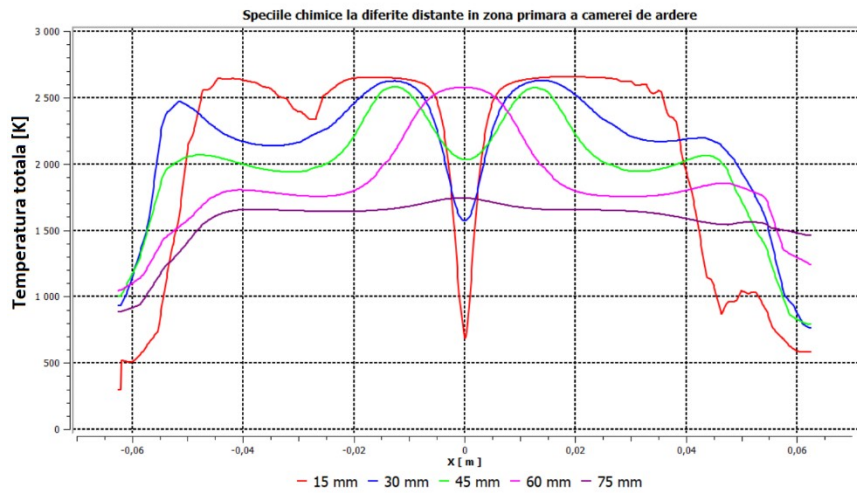


Figure 3.18 Total temperature evolution in the primary area of the calculation domain

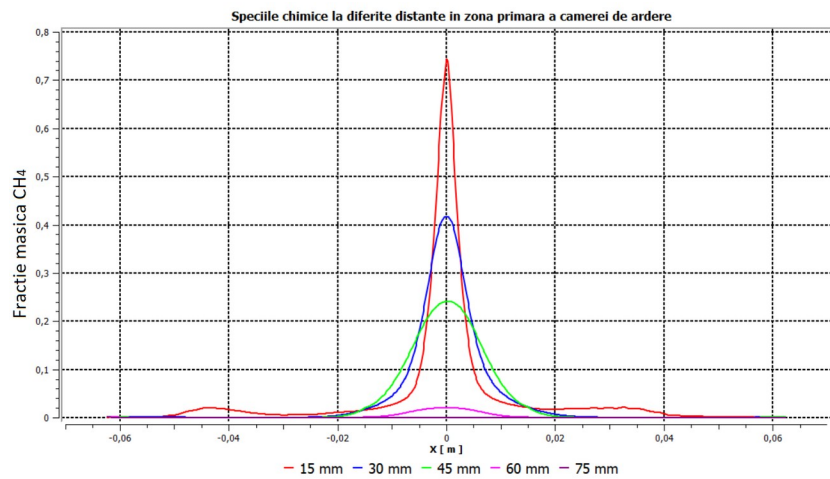


Figure 3.19 Evolution of the mass fraction of  $\text{CH}_4$  in the primary zone of the calculation domain

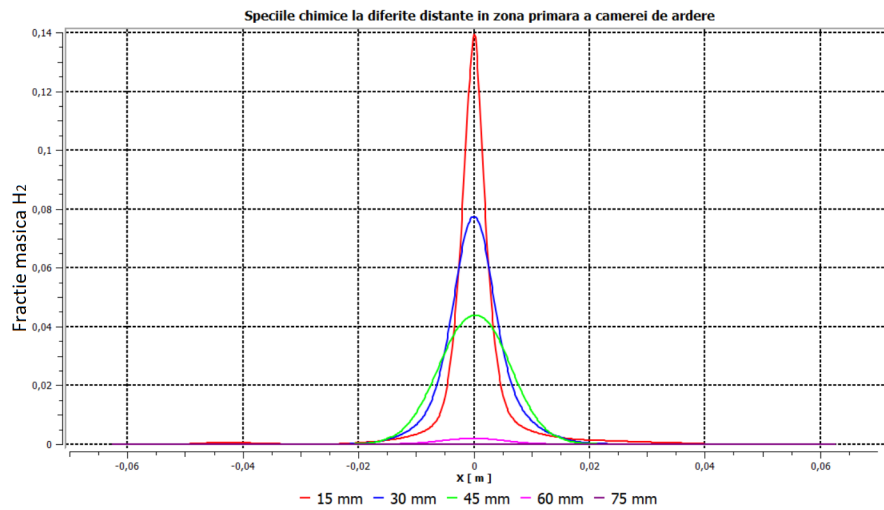


Figure 3.20 Evolution of the mass fraction of H<sub>2</sub> in the primary area of the calculation domain

From Figures 3.19-3.20, a larger mass fraction of CH<sub>4</sub>/H<sub>2</sub> mixture can be observed on the symmetry axis of the fire tube. Thus, most of the fuel mixture is injected into the fire tube through the central hole on the face of the swirler. Also, as we move away from the injector, the mass fractions of CH<sub>4</sub> and H<sub>2</sub> decrease. They reach the value 0 at a distance of 75 mm from the injector, suggesting a complete combustion of the fuel mixture.

#### 4. Conclusions

The research presented in this thesis had as its main aim the investigation and optimization of combustion processes in turbo-engines that use mixtures of methane and hydrogen. The results obtained from experimental campaigns and numerical simulations have made important contributions in the field of emission control and combustion stability for gas turbines, contributing to effective solutions for achieving energy sustainability objectives and reducing polluting emissions.

##### 1. Combustion efficiency in methane and hydrogen mixtures

One of the most relevant results of the study is related to the efficiency of combustion in mixtures of methane and hydrogen. It was found that with the increase in the volume percentage of hydrogen in the fuel mixture, the combustion efficiency increased considerably. In particular, for mixtures with a content of 60% and 80% H<sub>2</sub> they demonstrated a significant reduction in carbon monoxide (CO) emissions, due to the fact that hydrogen burns more quickly and completely compared to methane and that from an energetic point of view these mixes contain less carbon. In configurations tested with 60% H<sub>2</sub> in the fuel mixture, CO emissions were reduced by up to 50% compared to burning pure methane. This result is in accordance with the observations in the literature, according to which hydrogen allows complete oxidation due to the

higher flame propagation speed and higher temperature in the reaction zone. Furthermore, the flames generated in these mixtures were more compact and stable, favoring efficient combustion.

## **2. NO<sub>x</sub> emissions and the influence of flame temperature**

Another important aspect of the research was the assessment of NO<sub>x</sub> emissions, a major pollutant in gas turbines. As the volume proportion of hydrogen in the mixture increased, NO<sub>x</sub> emissions tended to increase, particularly due to the high flame temperature. For example, for 60% H<sub>2</sub> mixtures, NO<sub>x</sub> emissions increased by about 15-20% compared to pure methane mixtures. This increase is the result of the Zeldovich mechanism, responsible for the formation of thermal NO<sub>x</sub> at high temperatures. However, the use of innovative technical solutions, such as porous copper screen and swirl slots, allowed a significant reduction in NO<sub>x</sub> emissions. In the copper screen configuration, NO<sub>x</sub> emissions were reduced by up to 10% due to a more even distribution of oxidizer and fuel, which reduced high local temperatures in the combustion zone. The swirl slots contributed to better dilution of the mixture, reducing the formation of NO<sub>x</sub> when using mixtures with a high hydrogen content.

## **3. Flame stability and acoustic behavior**

One of the main objectives of the study was to investigate the flame stability during the combustion of hydrogen and methane mixtures. Hydrogen mixtures exhibited a more compact and intense flame due to the higher flame propagation speed and high energy release rate. This feature was particularly evident in the 80% H<sub>2</sub> mixtures, where the flame was more stable under high temperature conditions, having a reduced size compared to flames generated by pure methane. Regarding the acoustic disturbances, hydrogen-rich mixtures generated stronger acoustic pulsations, due to the higher flame temperature and implicitly the speed of sound propagation in the combustion gas environment. In particular, with 60% H<sub>2</sub> mixtures, acoustic pulsations of over 140 dB have been recorded, which can have a significant impact on swirler component life and overall system safety. However, the use of porous copper screen significantly reduced the noise level, by up to 8 dB in certain configurations and certain fuel mixtures. This solution has proven to be extremely effective in noise mitigation and can be implemented in gas turbines on an industrial scale.

## **4. Optimizing the geometry of the combustion chamber**

The geometry of the combustion chamber was a key factor in achieving optimal results in terms of combustion stability and emission reduction. The changes brought about by the use of swirl slots contributed to a more uniform distribution of the fuel-air mixture in the combustion chamber, which led to a reduction in local temperatures and implicitly to a decrease in NO<sub>x</sub>

formation. Additionally, these changes allowed for more stable flame operation, even under 100% H<sub>2</sub> conditions, where thermal instabilities and acoustic pulsations are normally harder to control. Experimental tests performed on configurations with axial fuel injection feeding the diffusive flame have shown a significant improvement in combustion stability with a reduction in sound pressure level. In particular, the swirl slots allowed for a more uniform flow and better dilution of the gases, ensuring a more efficient and controlled combustion process from the perspective of pollutant emissions from the flue gases. Compared to the initial configurations, the optimization of the combustion chamber geometry [C3] allowed stable operation even at high hydrogen concentrations, indicating the viability of this solution for industrial applications.

## **5. Viability of technical solutions for industrial applications**

The technical solutions tested in this research, such as porous copper screen, swirl slots and axial injection, have shown significant potential for their implementation in high-capacity gas turbines. These solutions not only contributed to the reduction of NO<sub>x</sub> and CO emissions, but also enabled the effective control of acoustic instabilities and thermal pulsations, thus ensuring a safe and efficient operation of the combustion system. The applicability of these solutions in industrial environments is supported by combustion stability and significant noise reduction, which are critical factors in the long-term operation of gas turbines.

The research carried out in this PhD thesis demonstrated the viability of using hydrogen as an alternative fuel (energy vector) for gas turbines, especially in a mixture with methane. The technical solutions proposed, such as the swirl slots, the copper screen and the axial fuel injection, allowed the optimization of the combustion process, the reduction of NO<sub>x</sub> and CO emissions, and the improvement of flame stability. These results may open new perspectives for the development of more efficient and environmentally friendly gas turbines, helping to reduce global emissions and increase energy efficiency in the industrial and energy sectors.

## **5. Personal Contributions and Dissemination**

### **5.1 Personal contributions**

The doctoral research materialized in a series of original contributions that used the theoretical, numerical and experimental research presented in the previous chapters. These personal contributions are summarized as follows :

- **Design and development of a new concept swirling combustion chamber for noise reduction** - One of my major contributions was the development of an innovative combustion chamber prototype that uses advanced premixing and swirling techniques. This combustion chamber has been specially designed to reduce the noise generated during combustion by

optimizing the swirler geometry and the air-fuel flow. By using helical blades in the swirler, a much more stable and compact combustion was achieved, which significantly reduced acoustic oscillations. Noise was reduced not only by better homogenization of the fuel-air mixture, but also by adjusting the geometric characteristics of the combustion chamber, which reduced acoustic pulsations and eliminated some of the aerodynamic instabilities caused by turbulent flow. This realization led to the filing of an invention patent at OSIM to patent the proposed, designed solution.

- **Experimental campaign focused on noise reduction in combustion processes -**

Another important aspect of my contribution consists in carrying out a detailed experimental campaign within the *National Research and Development Institute for Gas Turbines COMOTI*, where I investigated the combustion processes of methane and hydrogen mixtures. In experimental tests, we analyzed the acoustic frequencies generated during combustion using Fourier analysis and other advanced noise measurement methods. Experimental results showed a significant reduction in the noise level when burning hydrogen-enriched methane mixtures, especially at concentrations of 40% H<sub>2</sub> and 60% CH<sub>4</sub>. This configuration led to more stable combustion with reduced acoustic pulsations and a more compact flame, resulting in minimized sound oscillations and pressure fluctuations.

- **Numerical modeling to optimize noise reduction**

Another important pillar of my contribution consists in the realization of three-dimensional numerical simulations for the optimization of the reactive flow and the validation of an extended reaction mechanism for the combustion of hydrogen-enriched methane gas mixtures in the combustion chamber. Through numerical simulations, we identified technical solutions that allowed not only the stabilization of the flame, but also the reduction of thermoacoustic phenomena that generate noise. Following the simulations, we proposed adjusting some parameters such as the dimensions of the swirl slots and the fuel injection speed, which had a positive impact on the noise reduction. These optimizations were later validated in the experimental campaign, confirming the good correlation between the numerical modeling and the results obtained in reality.

- **Ensuring the compliance of pollutant emissions with the legislation in force**

Another important aspect of my research was the analysis of the pollutant emissions generated by the combustion of methane and hydrogen mixtures, in accordance with the current legal requirements for emissions of CO<sub>2</sub>, NO<sub>x</sub> and other pollutant gases. By using fuel mixtures containing up to 100% hydrogen, I managed to bring NO<sub>x</sub> and CO emissions (for methane-



hydrogen mixtures) to levels that respect the limits imposed by European and international legislation.

## **6. Future research directions**

As technology advances and emissions reduction requirements increase, research on optimizing combustion processes in turbo engines using alternative fuels, such as methane and hydrogen blends, continues to be essential. The present study proposes several future research directions to expand current knowledge and applications, thus ensuring an effective transition to cleaner and more sustainable energy sources.

### **1. Optimizing the geometry and configuration of the swirl injector**

A promising research direction is the optimization of the geometry and configuration of the swirler injector used in combustion chambers. Swirler blades geometry directly influences flame stability, air-fuel mixture efficiency, and pollutant emissions. Therefore, a detailed investigation of different blade configurations, including their angle, size and distribution, could provide innovative solutions to improve combustion performance. The use of advanced CFD numerical modeling and experimental laser measurement methods such as "Doppler global velocimetry (DGV)" could be beneficial for understanding the complexities of turbulent flow and flame behavior.

### **2. Study of combustion with alternative fuel mixtures**

In addition to using mixtures of methane and hydrogen, future research should explore the use of other alternative fuels, such as biogas or syngas, in combination with hydrogen. In-depth analysis is needed to assess how the physicochemical characteristics of these mixtures influence combustion parameters such as flame speed, combustion temperature, pollutant emissions and flame stability.

### **3. Development of advanced numerical modeling methods**

To improve the understanding of complex combustion processes, future research should include the development and implementation of more advanced Computational Fluid Dynamics (CFD) methods, such as LES (Large Eddy Simulation) and DNS (Direct Numerical Simulation). These methods allow a more detailed knowledge of reactive turbulent flows and associated phenomena such as autoignition or flashback. It could also be beneficial to integrate complex chemical models that accurately simulate the multiple reactions and thermochemical interactions during the combustion of methane and hydrogen mixtures.

### **4. Implementation of technologies for reducing emissions**

Reducing NO<sub>x</sub> emissions is a major challenge in hydrogen combustion due to high flame temperatures. Future research directions should include in-depth studies on rapid and uniform fuel-air mixing techniques to avoid areas of high local temperatures that favor NO<sub>x</sub> formation. In addition, the use of after-treatment technologies such as selective NO<sub>x</sub> reduction (SCR) catalysts could be explored to remove NO<sub>x</sub> from exhaust gases. Another important direction is the optimization of the combustion process by adjusting the fuel-air equivalence ratio and the use of innovative geometric configurations of combustion chambers that allow a more uniform distribution of the flame temperature. The use of dual or staged fuel injection technologies can help control NO<sub>x</sub> emissions by ensuring more complete and efficient combustion.

### **5. Investigation of Dynamic Flame Stabilization**

Another important research area is the investigation of dynamic flame stabilization under variable combustion conditions. Hydrogen-based flames have a different dynamic behavior than natural gas-based ones due to higher propagation speeds and local heat release rates. Future research should focus on analyzing the thermodynamic behavior of these flames, using analytical modeling techniques and advanced experimental methods to develop strategies to mitigate thermoacoustic pulsations, thereby ensuring stable operation of the combustion system.

### **6. Integration of combustion systems in renewable energy networks**

In the context of increasing the proportion of renewable sources in the energy system, it is important to investigate how fuel-switchable combustion systems can be efficiently integrated into modern energy networks. Future research could explore the impact of these systems on grid stability and energy efficiency, thus contributing to the transition to a low-carbon industry.

### **7. Development of New Materials and Technical Solutions for Hydrogen Combustion**

Hydrogen, through its unique combustion characteristics, imposes specific requirements on the materials used in turbo engine components. It is essential to develop new high temperature and corrosion resistant materials that can withstand reactive environments and intense duty cycles. Research should focus on evaluating different alloys and composite materials, as well as developing technical solutions to extend the life of critical components.

## 7. References:

- [1] RO137923A0, Cameră de ardere cu preamestec, turbionare și diluție primară, Enache, Marius Ștefan Prisețaru, Tudor Silivestru, Valentin CÂrlĂnescu, RĂzvan Mangra, Andreea Cristina Florean, Florin Gabriel Kuncser, Radu Eugen ,RO-BOPI 1/2024, [https://www.osim.ro/images/Publicatii/Inventii/2024/bopi\\_inv\\_01\\_2024.pdf](https://www.osim.ro/images/Publicatii/Inventii/2024/bopi_inv_01_2024.pdf)
- [2] Nam J., Lee Y., Joo S., Yoon Y., Yoh J.J., Numerical analysis of the effect of the hydrogen composition on a partially premixed gas turbine combustor, *Int. J. Hydrog. Energy*, vol. 44, pp. 6278–6286, 2019. <https://doi.org/10.1016/j.ijhydene.2019.01.066>.
- [3] Adam J. Gee , Douglas B. Proud , Neil Smith , Alfonso Chinnici , Paul R. Medwell, Hydrogen addition to a commercial self-aspirating burner and assessment of a practical burner modification strategy to improve performance, *International Journal of Hydrogen Energy*, <https://doi.org/10.1016/j.ijhydene.2023.06.230>
- [4] Zaiguo Fu, Lichao Sui, Jin Lu, Jiang Liu, Peifen Weng, Zhuoxiong Zeng, Weiguo Pan, Investigation on effects of hydrogen addition to the thermal performance of a traditional counter-flow combustor, *Energy*, vol. 262, Part A, 2023, 125465, <https://doi.org/10.1016/j.energy.2022.125465>
- [5] Abdelhalim A., Abdelhafez A., Nemitallah M.A., Effects of non-premixed H<sub>2</sub> injection on the stability, shape, and combustion/emissions characteristics of premixed CH<sub>4</sub>/air flames: An experimental study, *Fuel*, vol. 365, 2024, 131213, <https://doi.org/10.1016/j.fuel.2024.131213>
- [6] Marragou S., Magnes H., Poinot T., Selle L., Schuller T., Stabilization regimes and pollutant emissions from a dual fuel CH<sub>4</sub>/H<sub>2</sub> and dual swirl low NO<sub>x</sub> burner, *International Journal of Hydrogen Energy*, Vol. 47, Issue 44, pp 19275-19288, 2022, <https://doi.org/10.1016/j.ijhydene.2022.04.033>
- [7] Laera D., Agostinelli P.W., Selle L., Cazères Q., Oztarlik G., Schuller T., Gicquel L., Poinot T., Stabilization mechanisms of CH<sub>4</sub> premixed swirled flame enriched with a non-premixed hydrogen injection, *Proceedings of the Combustion Institute*, vol. 38, Iss. 4, pp 6355-6363, 2021, <https://doi.org/10.1016/j.proci.2020.06.378>
- [8] R. Carlanescu, Cercetari numerice si experimentale asupra efectelor adaugarii de hidrogen in gazul metan, in camera de ardere a unei turbine cu gaze, Teza Doctorat, Scoala Doctorala: inginerie Mecanica si Mecatronica, Universitatea Politehnica Bucuresti, 2018
- [9] S.B. Pope, "Turbulent Flows", Cambridge University Press, Cambridge, U.K., 2000
- [10] C.M. Müller, N. Peters, Reduced kinetic mechanisms for premixed methanol flames, in: N. Peters, B. Roog (Eds.), *Reduced Kinetic Mechanisms for Applications in Combustion Systems*, in: *Lecture Notes in Physics*, Springer-Verlag, Berlin, 1993, pp. 142–155.
- [11] Warnatz, J. "Rate coefficients in the C/H/O System, Chapter 5 in *Combustion Chemistry* (W.c. Gardiner Jr., ed.) Springer-Verlag, New York, pp 197-360, 1984
- [12] Yilmaz, H., Cam, O., Tangoz, S., Yilmaz, I., (2017). *Int J of Hydrogen Energy*, 42(40), 25744-25755.
- [12] Agarwal, A., Pitso, I (2020). *Materials Today: Proceedings*, 27(2), 1341-1349
- [13] Andreea Cristina Mangra, Razvan Carlanescu, Marius Enache, Florin Florean, Radu Kuncser, Numerical and experimental investigation of a micro gas turbine combustion chamber, *International Journal of Modern Manufacturing Technologies*, 2022, № 3, p. 139-145 <https://doi.org/10.54684/ijmmt.2022.14.3.139>